N78-32858

February 13, 1978 SC5094.25FPR

1.06 OPTICAL RECEIVER

Final Project Report

by

L.R. Tomasetta, H.D. Law, K. Nakano, F.W. Scholl, J.S. Harris, Jr.

Prepared under Contract No. NAS5-23862

by

ROCKWELL INTERNATIONAL SCIENCE CENTER
Thousand Oaks, California 91360

For

National Aeronautics and Space Administration
Greenbelt, MD 20771

Approved by:

J. S. Harris
Program Manager

Rockwell International
Science Center

UNCLASSIFIED

SECURITY CLASSIFICATION OF THIS PAGE *(When Data Entered)*

REPORT DOCUMENTATION PAGE		READ INSTRUCTIONS BEFORE COMPLETING FORM
1. REPORT NUMBER	2. GOVT ACCESSION NO.	3. RECIPIENT'S CATALOG NUMBER
4. TITLE *(and Subtitle)* 1.06 OPTICAL RECEIVER		5. TYPE OF REPORT & PERIOD COVERED Final Project Report Draft 01/28/77 thru 01/27/78
		6. PERFORMING ORG. REPORT NUMBER SC5094.25FPR
7. AUTHOR(s) L. R. Tomasetta, H. D. Law, K. Nakano, F.W. Scholl J. S. Harris		8. CONTRACT OR GRANT NUMBER(s) NAS5-23862
9. PERFORMING ORGANIZATION NAME AND ADDRESS Rockwell International Science Center 1049 Camino Dos Rios Thousand Oaks, CA 91360		10. PROGRAM ELEMENT, PROJECT, TASK AREA & WORK UNIT NUMBERS
11. CONTROLLING OFFICE NAME AND ADDRESS National Aeronautics & Space Administration Goddard Space Flight Center Greenbelt, Greenbelt, MD 20771		12. REPORT DATE February 13, 1978 13. NUMBER OF PAGES 78
14. MONITORING AGENCY NAME & ADDRESS *(if different from Controlling Office)*		15. SECURITY CLASS. *(of this report)* Unclassified 15a. DECLASSIFICATION/DOWNGRADING SCHEDULE

16. DISTRIBUTION STATEMENT *(of this Report)*

Approved for public release; distribution unlimited.

17. DISTRIBUTION STATEMENT *(of the abstract entered in Block 20, if different from Report)*

18. SUPPLEMENTARY NOTES

19. KEY WORDS *(Continue on reverse side if necessary and identify by block number)*

GaAlAs
GaAlSb
Avalanche Photodiode
Liquid Phase Epitaxy
Laser Rangefinding

20. ABSTRACT *(Continue on reverse side if necessary and identify by block number)*

The major conclusions of this work are: (1) that high performance 1.06μm avalanche photodetectors can be fabricated in the GaAlSb system. These devices have high quantum efficiency (90%), high speed (risetime < 60 ps) and low leakage currents (< 50 na). The dark current represents more than an order of magnitude reduction compared to previously reported results. The high speed avalanche gain of these devices is between 20 and 50. The area uniformity is better than ± 10%. (2) GaAlAs APDs at 0.53μm have even faster

DD FORM 1 JAN 73 1473 EDITION OF 1 NOV 65 IS OBSOLETE

UNCLASSIFIED

SECURITY CLASSIFICATION OF THIS PAGE *(When Data Entered)*

speed (risetimes $\sim$ 35 ps), lower dark currents ($\leq$ 10 pa) and high speed gains of 100-200. (3) Optical rangefinders based on measured III-V APD performance parameters have far superior performance when compared to even ideal PMTs in either a one color or two color rangefinder system.

For a one color system, f factor of two lower time jitter can be achieved with identical transmtited power. While for the two color receiver nearly an order of magnitude more transmitted power is required for the PMT receiver system to reach a 30 ps time jitter level. The superiority of the APD based two color receiver is significant and exists in the entire range of desired time jitters (< 100 ps) and received power levels.

TABLE OF CONTENTS

LIST OF ILLUSTRATIONS

Page

LIST OF ILLUSTRATIONS (Cont'd)

1.0 INTRODUCTION AND SUMMARY

This report describes progress towards realization of a high sensitivity optical receiver for precision rangefinding. The overall objective is to obtain 2 cm accuracy with 10-100 received photons. These requirements are based on current NASA efforts to develop a spaceborne rangefinder for geodetic survey. Evaluation of existing detector technologies, Si APDs and cross field photomultipliers indicated that a new receiver approach is required if the NASA requirements are to be met with a minimum of transmitted power. The III-V alloy avalanche photodetectors (APDs) are the only devices that have the very high speed ($t_r < 50ps$), and the very high quantum efficiency (>90%) to meet NASA's requirements. Principle efforts in the present contract were focused on improving the performance of 1.06μm avalanche photodiodes developed in part under NASA Contract NAS5-22806, providing a suitable high performance III-V alloy APD for doubled Nd:Yag at 0.53μm and analyzing the performance of receivers built with these detectors. These efforts resulted in 0.53μm APDs with greater than 90% quantum efficiency, dark currents of less than 10pa, uniform microwave avalanche gains of >100, pulse risetime of less than 40ps and pulse widths (FWHM) of less than 100ps. These devices are by far the fastest APDs ever reported in the 0.45μm to .90μm range. The 1.06μm APDs developed under this contract were a significant improvement over previous results at 1.06μm. The high quantum efficiency (>90%) previously obtained was now combined with uniform microwave avalanche gains of 30 (a factor of 10 increase in gain in addition to the elimination of hot spots, edge effects and microplasmas that previously

plagued these devices), the dark current was reduced by more than an order of magnitude for the best devices from 1μa to less than 50na. These photodiodes represent a significant achievement in APD technology and when combined with preamplifier configurations which fully exploit the incredibly low capacitance (0.2pf) of the devices represent the state-of-the-art in either 0.53μm or 1.06μm high speed optical receivers.

Under previous contract work with NASA and Air Force support (Air Force Contract F33615-74-C-1030, NASA Contracts NAS5-33333 and NAS5-23134) we have successfully demonstrated the 1.06μm receiver concept by the design and fabrication of hybrid integrated GaAs FET transimpedence amplifier receivers. These APD receivers showed a pulse sensitivity of 379 photons at 1.06μm (peak output voltage = rms noise output voltage) with a 10-90% risetime of 250ps and unity gain. These receivers demonstrated that the rangefinder goals could be met if photodiodes of sufficient avalanche gain (>20) could be produced. This was the principle thrust behind the work reported here.

The key factor in avalanche photodiode development is material quality; thus most of the program effort was devoted to improving doping control and eliminating interface defects which degrade gain uniformity and increase dark current. The GaAlSb and GaAlAs alloys were of greatest interest for 1.06μm and 0.53μm APDs, respectively. Improvements in gain, uniformity and dark current were sought and achieved. Suitable epitaxial growth procedures were developed for the fabrication of high quantum efficiency, low capacitance heterojunction device designs. Improved processing and packaging techniques were implemented. The APDs developed during the past year are, by far, the best high speed detectors in their wavelength range. These

detectors, when combined with state-of-the-art GaAs FET preamplifiers can indeed provide the best high speed optical receivers yet developed.

Calculations based on measured APD performance during its contract period show that for a one color system nearly a factor of two better time jitter performance can be achieved with an APD rangefinder than an ideal PMT receiver with identical transmitted power. For the two color case the advantages of an APD based receiver is even more impressive. In order to achieve a 50ps (1cm) time jitter, the PMT based system requires more than 5 times as much transmitted power. At lower time jitter levels (e.g. 30ps) the PMT based receiver required nearly an order of magnitude more transmitted power than an APD based system. This is a result of the nearly unity quantum efficiency of APD's, their greater speed and the fact that they can operate at the wavelength of transmitter while the PMT receiver, to operate at all, requires frequency doubling or tripling which results in a fewer number of transmitted photons for the same transmitted power.

2.0 PROGRAM GOALS AND TECHNICAL APPROACH

The objective of this program is to develop a 1.06μm optical receiver for precision rangefinding with 2 cm accuracy and 10-100 received photons. The immediate objective of this work is to develop high performance 1.06μm APDs which will be capable of providing the previously described optical rangefinder performance as well as a 0.53μm APD to complement the 1.06μm APD in two color rangefinder receiver systems.

The design goals of the APDs may be summarized: quantum efficiency 90%, 50Ω impulse response (FWHM) = 100ps; average avalanche gain = 30 gain uniformity ± 10% with an active optical diameter of 0.12mm. The APD requirements are determined by the details of pulse signal to noise ratio discussed in Section 2.1. The material and device design approaches are described in Sections 2.2 and 2.3. The receiver approach for a one color 1.06μm or 0.53μm receiver as well as a dual (1.06μm and 0.53μm) color receiver is discussed in Section 2.4

2.1 System Requirements

The overall objective of this program is to develop an avalanche photodiode receiver for NASA rangefinding applications. However, at the present time, very little practical experience with such a system is available. The purpose of the following analysis is to lay the foundation for determining the importance of the APD device parameters for rangefinder applications. The significant questions are: What parameters limit performance? Are the limitations fundamental to the approach being taken or

do they require only further device improvement? For nearly ideal amplifiers such as the PMT, range accuracy will be shot noise limited; this is, of course, the ultimate performance limit. Systems performance is then solely dependent on speed and quantum efficiency. Avalanche photodetectors, on the other hand, suffer from excess noise and time jitter, both intrinsic to the two-carrier gain process itself. These effects are expected to degrade the ultimate range accuracy to somewhat less than the shot noise limit. In addition, the usual thermal noise contribution to range error must be considered. Complete theoretical evaluation of all these noise sources is beyond the scope of this program but we do give a simplified discussion of range accuracy; considering first thermal and secondly quantum noise limitations.

Let us consider an optical receiver with an incident number of photons, N_{ph}, in a light pulse on the detector. If the quantum efficiency is η and the average avalanche gain is M, then the number of electrons flowing in the preamp input is

$$N_e = \eta M N_{ph} \tag{2.1}$$

and the total charge is

$$Q_p = q \eta M N_{ph}. \tag{2.2}$$

In general, such a charge pulse will produce an output voltage pulse from the

preamplifier, the peak value of which, V_p will be proportional to Q_p, i.e.,

$$V_p = \left(\frac{V}{Q}\right)_p Q_p \tag{2.3}$$

The constant of proportionality of "pulse gain", $(V/Q)_p$ will depend on the bandwidth characteristics of the receiver and the shape of the incident pulse. In the limit of an infinitely short (δ-function) incident current pulse into the preamp, there is a characteristic output pulse waveform $V_\delta(t)$ and pulse gain $(V/Q)_\delta$ which depends only on the preamplifier gain characteristics. The response V(t) to any arbitrary input current pulse, i(t) can be obtained from $V_\delta(t)$ by convolving i(t) with $V_\delta(t)$.

In addition to the signal output pulse, the preamplifier also exhibits some rms noise output voltage, v_{no}. If there were no output voltage noise then the receiver would give virtually unlimited time resolution when followed by a constant-fraction discriminator (CFD) (limited only by jitter in the CFD and time jitter in the detector itself - which is extremely small in any III-V APD's). If we are trying to measure a time t_o at which V(t) would cross some level V_o, then the effect of noise is to introduce an uncertainty in V(t) which at all times is given by some probability function. If we assume that the slope of V(t), $\frac{dV}{dt}$, is essentially constant over the region $V_o \pm 2\ v_{no}$, then the same uncertainty in when V(t) will actually cross V_o is given by the same shaped probability function as the voltage noise, only with the voltage horizontal scale replaced by voltage divided by

dV/dt. Hence, the rms time uncertainty, ΔT_{rms}, in V(t) crossing V_o is given by

$$T_{rms} = \frac{v_{no}}{\left(\frac{dV}{dt}\right)_{t = t_o}} \tag{2.4}$$

where v_{no} is the rms output noise.

The slope $(dV/dt)_{t=to}$ can be approximated by more commonly measured receiver parameters as

$$(dV/dt)_{t=t_o} = V_p/T_{PR}, \tag{2.5}$$

where T_{PR} is the pulse risetime. Substituting Eq.(2.5) in Eq.(2.4), we have

$$\Delta T_{rms} = \frac{v_{no}}{V_p} T_{PR}, \tag{2.6}$$

where it is assumed that V_p is considerably greater than v_{no} (the false alarm rate would obviously be unacceptably high if it were not, anyway). This expression can further be related to the preamplifier parameters discussed earlier by substituting Eq.(2.3), giving

$$\Delta T_{rms} = \frac{v_{no}}{\left(\frac{V}{Q}\right)_p \; Q_p} T_{PR} \tag{2.7}$$

or from Eqs.(2.1) and (2.2)

$$\Delta T_{rms} = \frac{v_{no} \quad T_{PR}}{q\left(\frac{V}{Q}\right)_p \quad N_e} \tag{2.8}$$

where $(V/Q)_p$ is the "pulse gain" and N_e the number of electrons flowing in the preamp input. The "minimum detectable current pulse" of the preamp, N_{op} is given by

$$N_{op} = \frac{v_{no}}{q\left(\frac{V}{Q}\right)_p} \tag{2.9}$$

N_{op} is just the number of electrons in a current pulse required to make the peak output voltage equal the rms output noise. In terms of N_{op} then, Eq.(2.8) becomes (assuming N_e considerably greater than N_{op})

$$\Delta T_{rms} = \frac{N_{op}}{N_e} T_{PR} \cdot \tag{2.10}$$

This can be expressed in terms of the number of photons in the light pulse, N_{ph}, the quantum efficienty, η, and average avalanche gain, M from Eq.(2.1) by

$$M_{MIN} = \frac{N_{op} \ T_{PR}}{N_{ph} \ T_{rms}} \tag{2.11}$$

or conversely using (2.8) and (2.1)

$$\Delta T_{rms} = \frac{v_{no}}{q\left(\frac{V}{Q}\right)_p} \quad \frac{T_{PR}}{\eta M N_{ph}} \tag{2.12}$$

In this form the various parameters of the detector and preamplifier can be separated and the importance of each determined. The principle "device only" parameters are M and η, the gain and quantum efficiency; $\left(\frac{V}{Q}\right)_p$ is the principle "preamp only" parameter and v_{no} and T_{PR} are dependent on both the preamp and APD. In general, the best receiver will have high quantum efficiency, η, short risetime, T_{PR}, and a large charge sensitivity, $\left(\frac{V}{Q}\right)_p$. Although a large gain, M, would also seem desirable, v_{no} and M are related through the excess multiplication noise and therefore a limit on M for the APD case will provide optimum receiver performance. Let us now examine the contributors to v_{no} for both the ideal PMT and APD case.

The noise current can be calculated in the usual way as follows:

$$i_n^2 = \frac{4KT}{R_f} \Delta f + (2\pi f e_n C)^2 \Delta f + 2qM^{2+x_n}\left(\frac{\eta q N_p}{\Delta T_o} + I_B\right)\Delta f \tag{2.13}$$

where R_f is the equivalent front end resistor,

e_n is the preamp voltage noise source,

x_n is the excess noise factor,

ΔT_o is the pulse width

I_B is the bulk dark current.

For the ideal PMT case $I_B = 0$ and $X_n = 0$. Therefore M can be made as large as possible so that

$$i_n^2 = \frac{2q^2M^2\eta N_p}{\Delta T_o} \Delta f \quad \text{for M large} \tag{2.14}$$

Since $v_{no} = R_f\, i_n$

$$\Delta T_{rms} = R_f \sqrt{\frac{2\eta N_p \Delta f}{\Delta T_o}} \quad \frac{T_{PR}}{q\left(\frac{V}{Q}\right)_p \eta N_p} = R_f \sqrt{\frac{2\Delta f}{N_p \Delta T_o \eta}} \quad \frac{T_{PR}}{\left(\frac{V}{Q}\right)_p} \tag{2.15}$$

The pulse sensitivity can be expressed in terms of the transimpedence and the pulse width,

$$\left(\frac{V}{Q}\right)_p = \frac{R_f}{\Delta T_o} \tag{2.16}$$

and since $2\Delta T_o = \frac{1}{\Delta F}$ (2.17)

$$\Delta T_{rms} = \sqrt{\frac{1}{N_p \eta}} \quad T_{PR} \tag{2.18}$$

Thus for an ideal PMT there are only two parameters critical to receiver performance: risetime and quantum efficiency. Best performance will be achieved with highest quantum efficiency and fastest risetimes.

For an APD the results are slightly more complicated since the excess avalanche noise is not zero. With careful choice of preamps (GaAs FETs in

this case) the excess voltage noise term can be neglected and the result expressed as

$$i_n^2 = \left[\frac{4KT}{R_f} + 2q\,M^{2+X_n}\left(\frac{q\eta N_p}{\Delta T_o}\right) + I_B\right]\Delta f \qquad (2.19)$$

$$V_{no} = R_f\sqrt{\left(\frac{4KT}{R_f} + 2qM^{2+X_n}\left(\frac{q\eta N_p}{\Delta T_o} + I_B\right)\right)\Delta f} \qquad (2.20)$$

$$\Delta T_{RMS} = \frac{T_{PR}\Delta T_o}{q\eta M N_p}\sqrt{\left(\frac{4KT}{Rf} + 2qM^{2+X_n}\left(\frac{q\eta N_p}{\Delta T_o} + I_B\right)\right)\Delta F} \qquad (2.21)$$

For the case when shot noise dominates Johnson noise and the dark current can be neglected, the result is

$$\Delta T_{rms} = T_{PR}\sqrt{\frac{M^{X_n}}{\eta N_p}} \qquad (2.22)$$

Comparing Eqs.(2.22) and (2.18) we see that the APD result is degraded by $M^{Xn/2}$. The question which now arises and forms the impetus for this development program is, "Can η and T_{PR} of III-V APDs be made sufficiently superior to state-of-the-art PMTs to provide a significant system performance advantage? The answer to the question is an unqualified yes. The details of the calcultions based on APD parameters measured as part of this program are contained in Section 3. The results show that the performance of a III-V APD receiver based on a 1.06μm Nd:Yag transmitter is superior to state-of-the-art PMTs in either a single color or dual color receiver configuration.

2.2 Materials Approach

The heterojunction III-V alloy materials technology provides the only viable approach to achieve suitable photodiodes for rangefinding at 1.06μm and 0.53μm. Figure 2.1 shows the bandgap and lattice constant of the principle binary III-V's and their alloys. For operation at 1.06μm (1.17 eV) we require an active absorbing layer with a bandgap of $\approx$1.1 eV. Smaller gap results in excess dark current; larger bandgap results in low quantum efficiency. GaAsSb, GaInAs, InGaAsP, and GaAlSb are the possibilities. Of these, only InGaAsP and GaAlSb can be grown on lattice matched substrates (InP and GaSb). At present, the precise doping control necessary for very high speed operation has not been demonstrated in InGaAsP. On the other hand, our previous work GaAlSb photocathodes had demonstrated that device quality multilayer structures with controlled doping could be fabricated from AlGaSb alloys. Thus, we elected to develop this material for 1.06μm photodiodes.

The experimentally determined AlGaSb band structure over the whole range of compositions is shown in Fig. 2.2.[1] This diagram is relatively well established except at the AlSb end, where the ordering of the X and L minima is still uncertain. For most of the alloy composition range, it is seen that AlGaSb is an indirect semiconductor with L (or X) conduction band minima. Fabrication of high performance heterojunction photodiodes requires two alloy layers: the first, active layer, must strongly absorb (~1-2μm absorption depth) at 1.064μm; the second, window layer, must have zero absorption at 1.064μm. Reference to Fig. 2.2 shows that alloys with 23-30% AlSb have suitable direct (Γ) minima for absorber layers, while those with 35-40% AlSb can serve as transparent window layers. The other details of the band structure are largely irrelevant to APD design. The actual separations

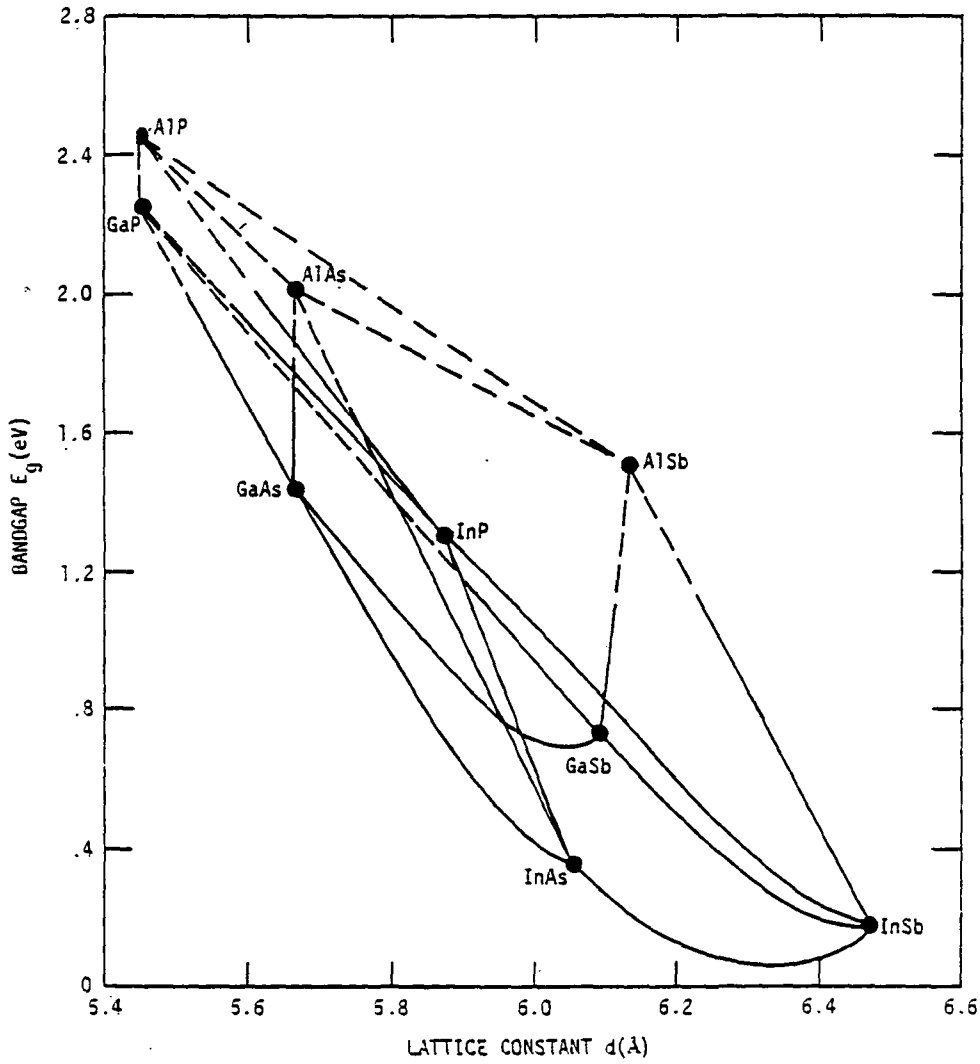

Fig. 2.1. Bandgap-lattice constant diagram for alloys of III-V semiconductors.

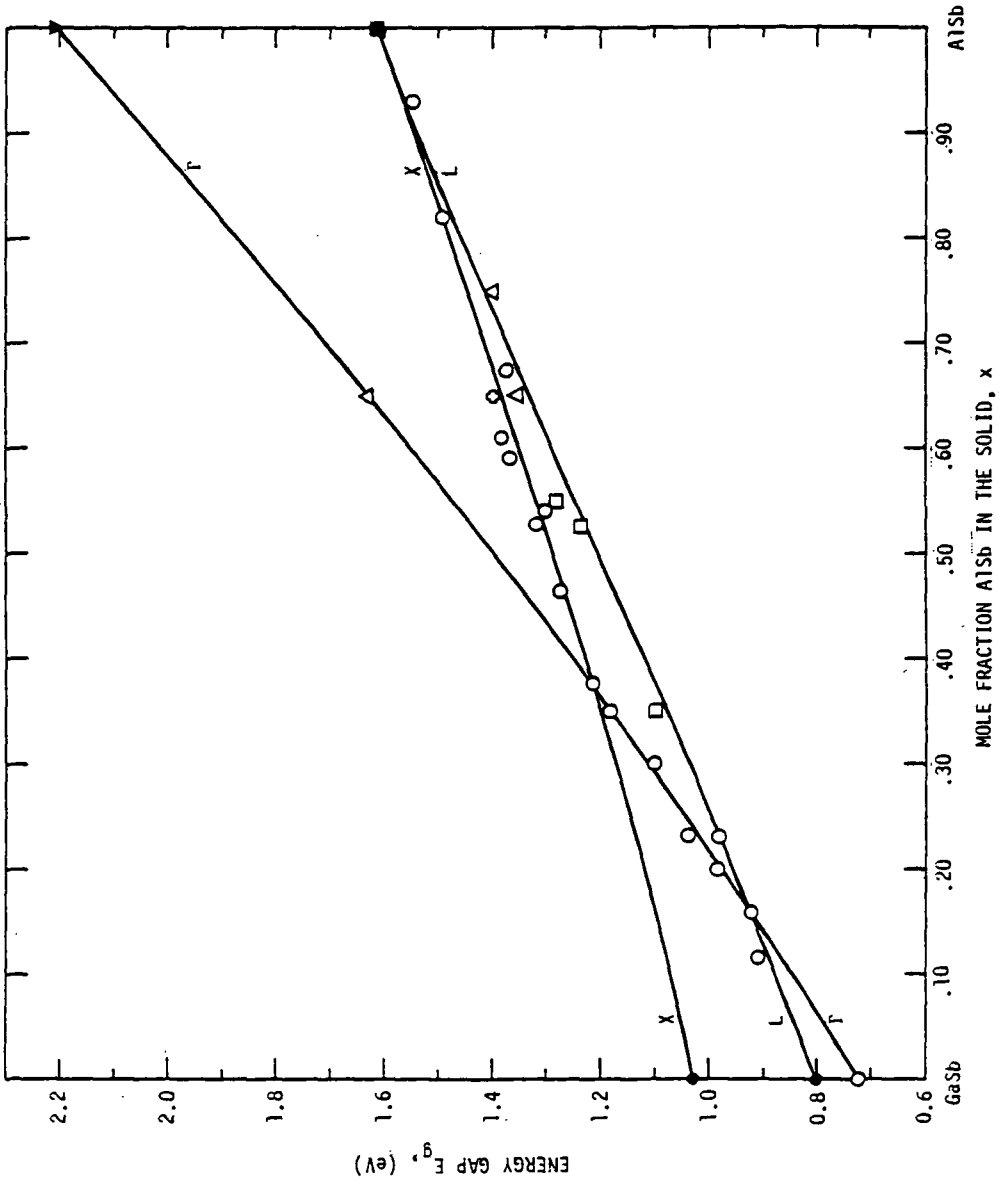

Fig. 2.2 AlGaSb Band Structure.

and orderings of the 3 non-equivalent conduction band minima may well influence the microscopic electron and hole ionization rates (discussed in Section 3), but the band structure obviously cannot be altered to provide more favorable avalanche gain.

2.3 Device Design

A suitable device structure may be based on the materials available. One such design is shown in Fig. 2.3. This structure contains (1) buffer layer of 11.5% AlSb, (2) field termination layer of p^+ $Ga_{.77}Al_{.23}Sb$, (3) active depleted layer of n^- $Ga_{.77}Al_{.23}Sb$, (4) window layer, transparent to 1.06μm, of $Ga_{.60}Al_{.40}Sb$. With suitable antireflection coating on the $Ga_{.60}Al_{.40}Sb$ surface virtually 100% of all incident photons can be rapidly (transit time $\sim 5\times10^{-4}cm/10^{7}cm/s$ = 50ps) collected by the n^- layer. This layer is fully depleted at operating bias. The parallel equipotentials and strong optical absorption ensure an rms transit time dispersion of less than $\frac{1}{\sqrt{2\alpha V_s}}$ = 7.07ps (at unity gain).

The device structure shown in Fig. 2.3 offers virtually 100% quantum efficiency, minimum excess multiplication noise, no diffusion tail or "back porch", and immunity to surface breakdown. At operating bias, as noted above, the n^- layer is fully depleted; thus all incident carriers immediately see the large junction potential. The resultant photocurrent is ideally "pure" in that it consists entirely of holes (in this case). This situation results in the least excess multiplication noise, assuming, of course, that $\beta > \alpha$ (β = hole ionization rate, α = electron ionization rate, both in cm^{-1}). If $\beta \leq \alpha$, obviously the complementary structure would be grown. The p^+/n^- layer

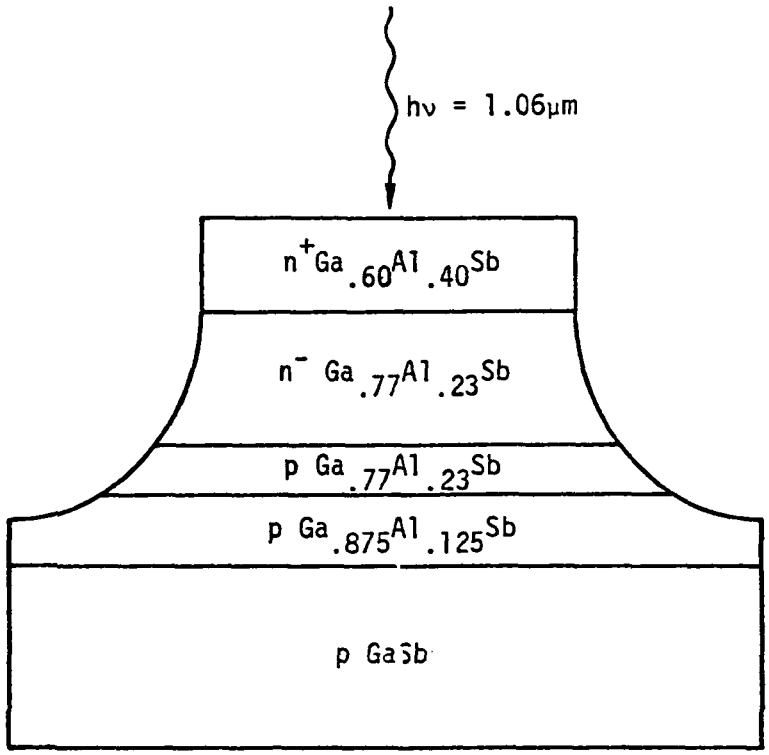

Fig. 2.3 AlGaSb APD Structure. Enough Al is added to top window layer to attain virtual 100% quantum efficiency.

sequence yields a device geometry which should be immune to surface breakdown. Mesa diodes have a cross section which increases as one moves away from the top surface of the mesa. This geometrical factor, combined with the layer sequence of Fig. 2.3, results in surface electric fields considerably lower than the bulk fields. Thus uniform bulk avalanche results.

2.4 Receiver Approach

The receiver approach used in the analysis conducted in Section 3 is based on the hybrid integration of GaAs FETs and III-V alloy APDs into a transimpedence feedback amplifier. This approach allows the very low capacitance of the APDs and FETs to be fully utilized by eliminating the stray capacitance of the package and leads that would substantially increase the capacitance of discrete packaged components were used. By keeping the capacitance as small as possible a larger feedback resistor can be used for the same frequency response and thus Johnson noise can be reduced and better preamp performance achieved. Details of the design will be discussed in the next section.

3.0 RESULTS

This contract work resulted in the best performance ever demonstrated for very high speed, very high quantum avalanche photodiode at 0.53μm and 1.06μm. This section describes the results of this APD development program as well as a system analysis of a rangefinder receiver based on these measurements.

3.1 GaAlAs 0.53μm APD Results

The major effort with regard to the GaAlAs, 0.53μm APDs was to improve the microwave avalanche gain, increase the speed and reduce the dark current of the device.

Improvements in low doping level control resulted in reducing leakage currents to the 1-10 pA range. Wafer processing and packaging techniques improved both the speed of the detector and the microwave avalanche gain.

Figure 3.1 shows the high speed response of the diode in the modified package. A frequency doubled mode locked Nd:Yag laser is used as the source of incident radiation. The 10-90% risetime is less than 40ps and the FWHM pulse width is 130ps. Figure 3.2 shows the schematic of the processed device structure.

Figure 3.3 shows photoresponse of the diode to a doubled, mode locked Nd:Yag laser operating at a repetition rate of 273 MHz. The top curve of Figure 3.3 shows the output of a spectrum analyzer set at 273 MHz with a 3 kHz resolution window with the mode locked laser, suitably attenuated, incident on the detector. The next curve shows the diode response with the laser operating but the beam blocked. This is a measure of the dark current.

NAS5-23862-SC5094.25FPR Fig. 3.1

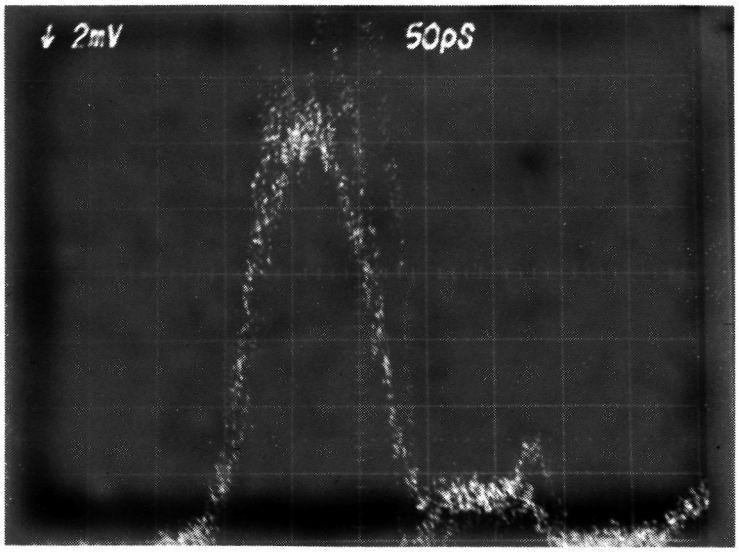

Fig. 3.1 GaAlAs/GaAs 0.53μm impulse response.

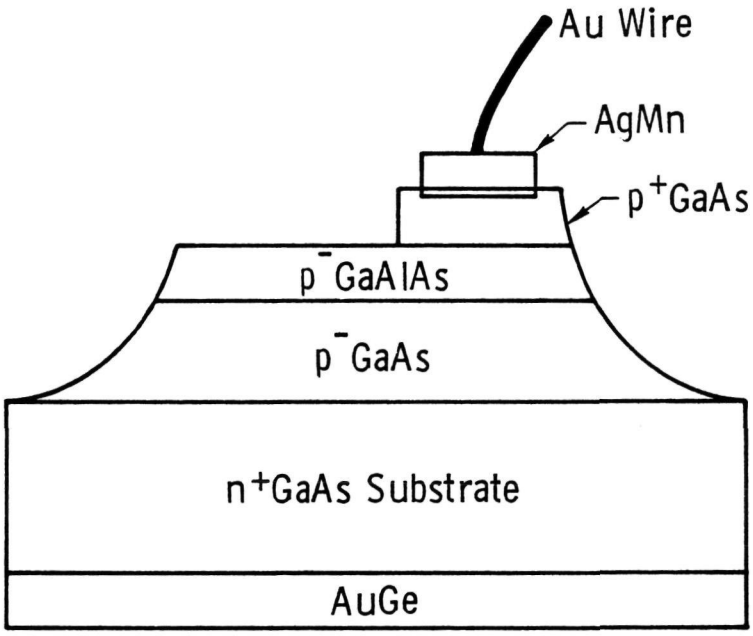

Fig. 3.2 GaAlAs/GaAs avalanche photodetecter.

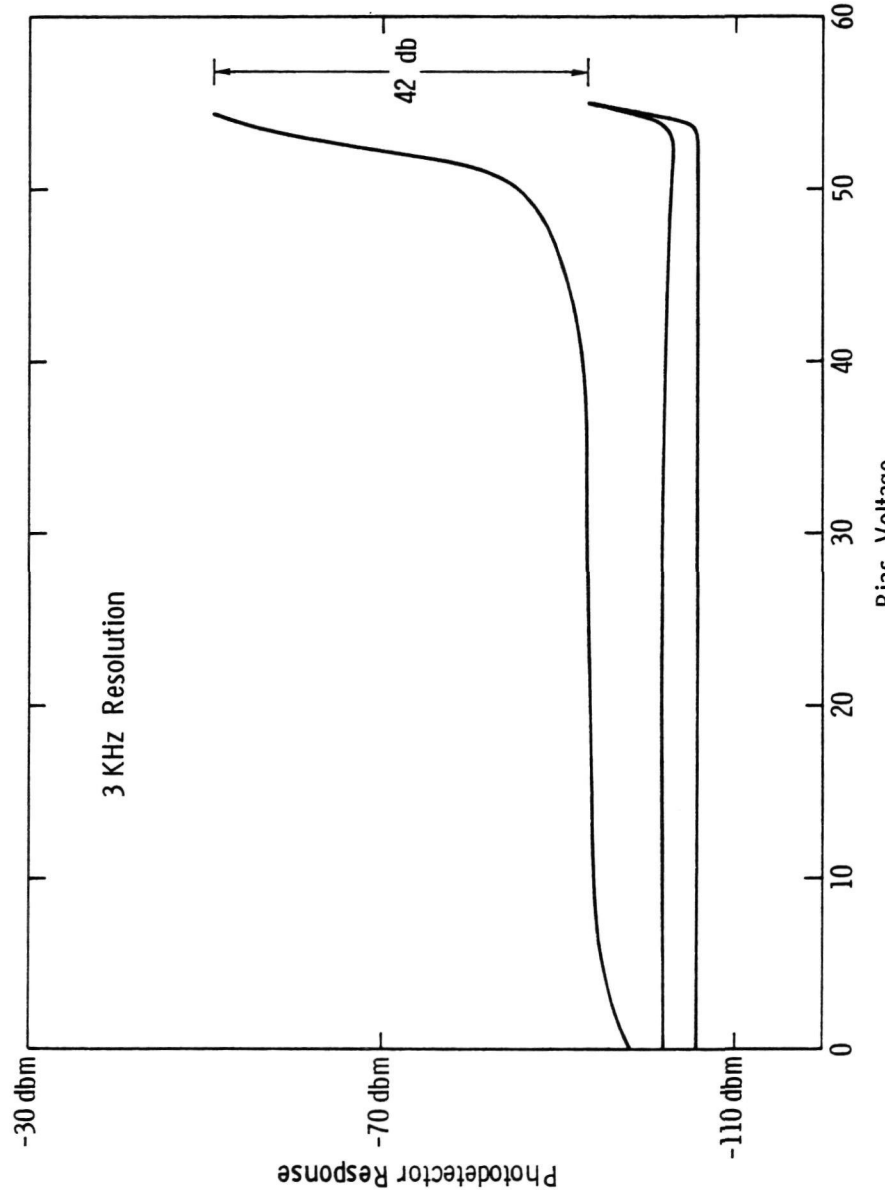

Fig. 3.3 High speed photoresponse of a GaAlAs/GaAs avalanche photodetector.

The lower curve shows the superimposed response of diode with and without incident radiation when the spectrum analyzer is tuned away from the 273 MHz repetition rate of the laser. The difference in the low bias levels is due to slight pickup from the electrical pulser used to drive the laser. The most significant item to notice is the fact that the microwave avalanche gain of the diode is nearly 100.

Table 1 summarizes the performance of 0.53 μm avalanche photodiode.

TABLE 1

0.53 μm Avalanche Photodetector Characteristics

I_R	> 90% @ 40 V < 0.1 na @ 40 V
M (high speed)	100 @ 55 V
t_r (10-90%)	< 40 ps
t_p (FWHM)	< 150 ps
diameter	75 μm

The complete data sheets supplied with the two 0.53μm APDs delivered under this contract are supplied in the appendix.

3.2 GaAlSb Materials Growth and Evaluation

The growth of GaAsSb for 1.06μm APD has been plagued by severe field non-uniformities, microplasmas and edge breakdown because of the severe substrate-epilayer lattice micmatch. Attempts to reduce this lattice match by growing a series of compensating buffer layers where part of the discontinuity is taken up at each of these buffer interfaces has improved the avalanche gain uniformity somewhat, but still not enough to meet the requirements of a state of the art APD.

Unlike the GaAsSb/GaAs system, the growth of GaAlSb on GaSb substrate has a fairly good lattice match. For the full range of x in $Ga_{1-x}Al_xSb$, the largest lattice mismatch is only 0.7%. For all the devices of interest here, $x < 0.5$ which limited the lattice mismatch to $< 0.35\%$.

The surface morphology of the epilayer in the GaAlSb system is superior to that of the GaAsSb. Figure 3.4 shows a typical surface as grown of a $Ga_{.55}Al_{.45}Sb$ layer. Comparing Fig. 3.4 with the GaAsSb surface shown in Fig. 3.5, the superiority of surface morphology in the GaAlSb layer is clearly evident.

One of the key elements of achieving good epitaxial growth is the surface preparation and removal of surface oxides immediately prior to growth. The substrate polishing in GaSb is not straightforward since the surface of the substrate is extremely sensitive to every step in polishing process prior to growth. Several methods work well in polishing the GaSb substrates. A carbosyl + H_2O_2 + H_2O polish on cloth after 3μm alumina grit lapping provides a mirror surface. However, this method leaves quite a large amount of mechanical damage which shows up under a 3% Br-CH_3OH etch. A better method which minimizes the polishing damage has been developed. A solution consisting of 1cc bromine, 800cc of methanol and 200cc of glycerol is used to polish the GaSb on a rotating disc. A higher percentage of bromine can be used at first to polish the substrate down to one mil greater than the desired thickness. Then, the above solution is used as the final polish. The 0.1% bromine solution was found to be the optimum solution. A higher percentage of bromine results in faster chemical etching action during polish and usually leaves rounded edges on the substrate. On the other hand, a lower

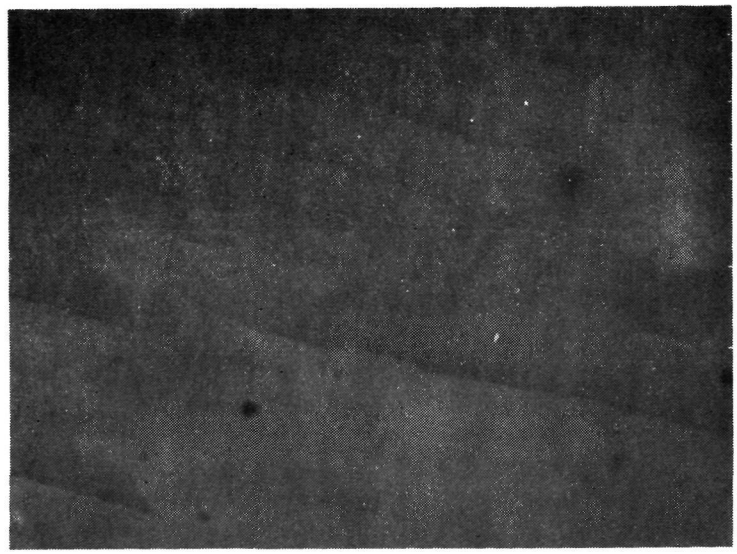

Fig. 3.4 Typical surface morphology of a $Ga_{.55}Al_{.45}Sb$ layer.

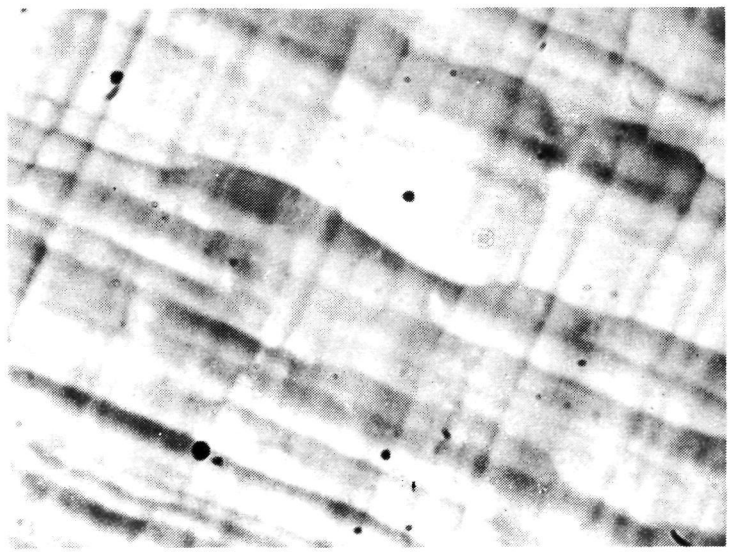

Fig. 3.5 Typical surface morphology of a $GaAs_{.85}Sb_{.15}$ layer.

percentage of bromine in the solution reduces the chemical etching and cause more mechanical damage on the substrate surface. The glycerol in the solution plays the role of an inert lubricant. A complex oxide, which is difficult to dissolve, can easily form on the polished surface of the GaSb substrates. This makes the sample preparation procedure prior to growth very critical. In order to get a good growth, these complexes must be prevented from forming during every wafer cleaning procedure. The polished substrate is boiled in trichloroethylene, acetone, methanol and isopropyl alcohol in that order. At no time is the sample exposed to air. After cleaning in solvents, the sample is blown dry by clean nitrogen. It is then put into HF for 5 minutes to remove all residual oxides. The HF is then quenched with methanol. The sample is etched in 2% bromine-methanol with constant agitation. A large amount of methanol is used to quench the etch so as to prevent exposure to air. The sample is finally rinsed in isopropyl alcohol, blown dry and immediately loaded into the furnace.

An equivalently good result is obtained by stripping the surface of the substrate by an anodic oxidation method. The polished GaSb substrate is solvent cleaned, and then is oxidized anodically. A low current density must be used in the oxidation process or the polished substrate will turn rough. The grown oxides are then stripped by concentrated HF solution and rinsed in isopropyl alcohol. This method considerably reduces substrate preparation time.

A second key element in the growth of GaAlSb is precise control over the degree of melt supersaturation during growth. In order to obtain good nucleation and resulting epitaxial growth, the GaAlSb melt must be supersaturated between 2^{o} and $4^{o}C$. This is especially critical for

GaAlSb because at approximately $5^{o}C$ supersaturation, polycrystal formation occurs in the bulk of the melt and all supersaturation is lost. The quick polycrystal formation is associated with the fast growth rate of this material. With no supersaturation, the ternary GaAlSb melt will etch back a GaSb substrate and very poor surface morphology and layer uniformity result. Thus, in multi-layer structures, each melt must be precisely equilibrated so that it has the exact degree of supersaturaton required for growth at the substrate temperature.

Since the growth rate of GaAlSb is so fast, it is essential to have a slow furnace cooling rate ($<0.2^{o}C$/min) to control the growth rate. The slower the growth rate, the less stacking faults will result. It has been experimentally determined that a slower cooling rate produces better epitaxial layers.

Since the degree of supercooling is so important to the GaAlSb growth, the liquidus is studied in detail. A semi-transparent furnace is used to determine the exact saturation temperature. Data points of this study are observed near $500^{o}C$ and the liquidus line at 490^{o}, 500^{o} and $510^{o}C$ are shown in Fig. 3.6.

The solid composition of the GaAlSb layers cannot be measured by the Gandolfi method due to the close lattice match. The resolution of the x-ray diffraction is not good enough for an accurate measurement. The percentage of AlSb in the solid is best measured by the microprobe method. Once a standard sample is available, the composition can be measured easily. The solidus curve is shown in Fig. 3.7.

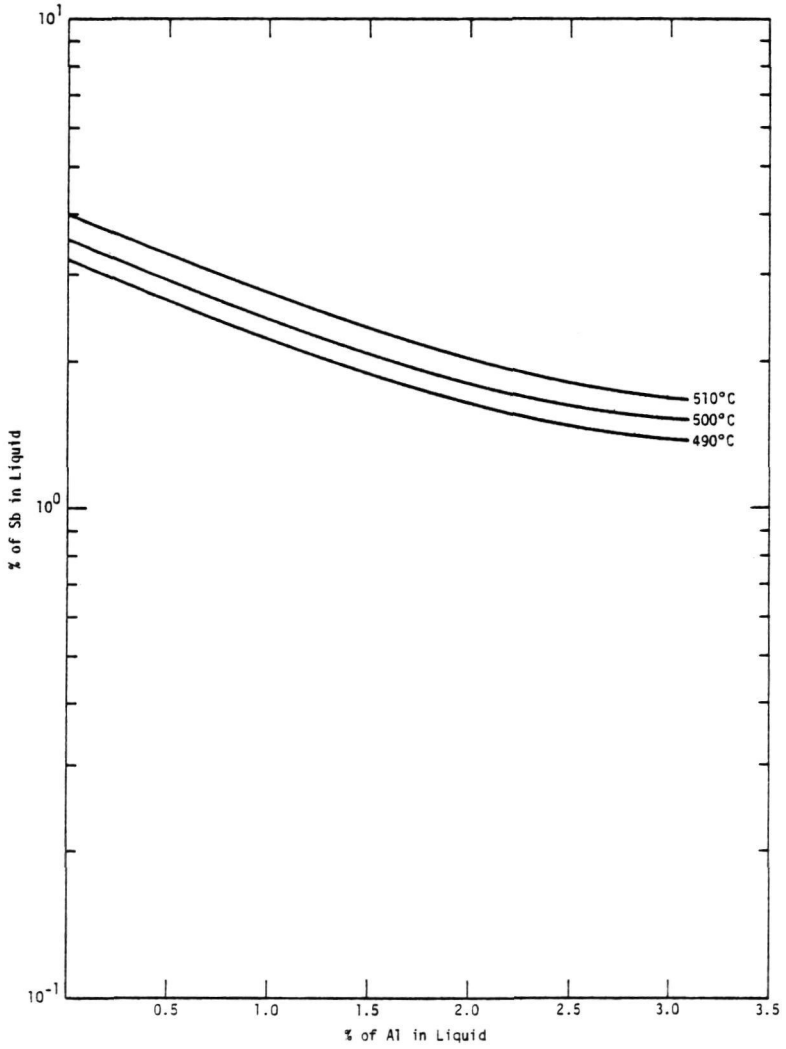

Fig. 3.6 Experimental liquidus curve of GaAlSb measured by a transparent furnace.

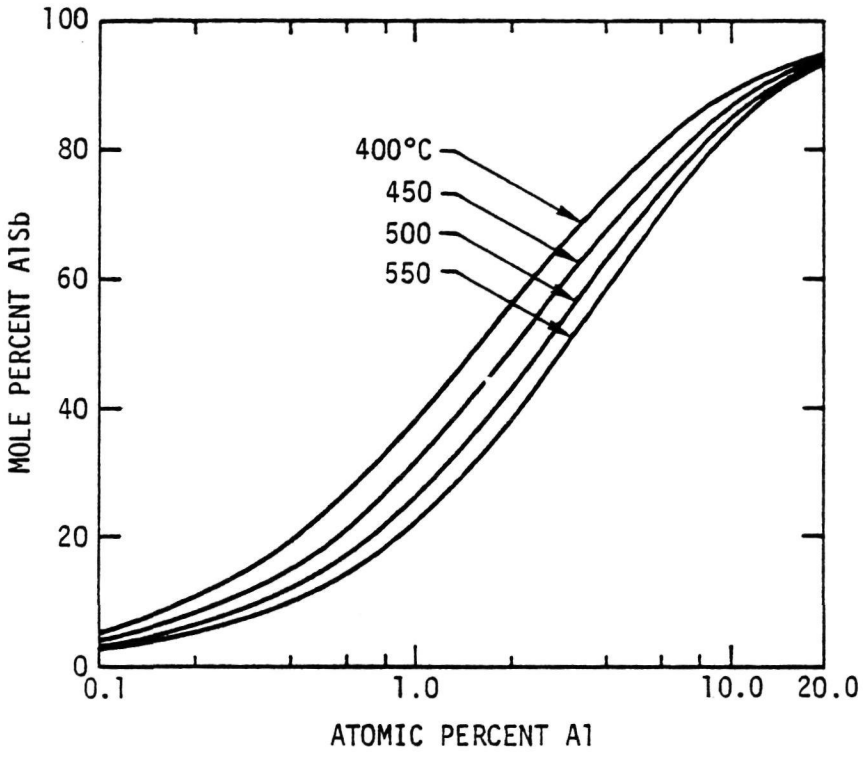

Fig. 3.7 Solidus of GaAlSb alloys.

The energy band of GaAlSb alloys was studied in this laboratory by Anderson et al.[1] GaSb is a direct bandgap material while AlSb is an indirect bandgap material. Therefore, a crossover should occur for some x in $Ga_{1-x}Al_xSb$. Figure 2.2 shows the band diagram of $Ga_{1-x}Al_xSb$. Beyond 18% of AlSb, the alloy is an indirect bandgap material. It does not seem that $Ga_{1-x}Al_xSb$ should have a high absorption coefficient at 1.06μm. However, for x = 0.26, Γ is just 0.028 eV above L. Therefore at 1.06μm, the direct bandgap dominates the absorption. This effect, moreover, reduces the ionization rate of electrons relative to holes. The implication of this ionization rate change will be discussed in the Device Performance section.

The absorption coefficients of several GaAlSb alloys are shown in Fig. 3.8. For $Ga_{.74}Al_{.26}Sb$, the absorption coefficient at 1.06μm is approximately equal to $10^4 cm^{-1}$. This will produce high quantum efficiency diodes at the desired 1.06μm wavelength.

At this point, it is obvious that GaAlSb system should be better than the GaAsSb for APD application. However, several improvements must still be made on the GaAlSb system to realize the advantages. The n-type GaSb susbtrate must be improved. The doping striations and damage shows up clearly when the substrate is etched in Bromine-methanol. This will have to be improved before a more uniform epitaxial layer can be grown. Also, the doping level control on the epitaxial layer should be improved. The undoped GaSb layers have a high concentration of Sb vacancies which turns the crystal to $1x10^{17} cm^{-3}$ p-type at room temperature. A very accurate compensation dopant is needed to produce epitaxial layer in the low $10^{15} cm^{-3}$ carrier concentration. Some success has been achieved with compensation experiments but better control should be possible with additional work.

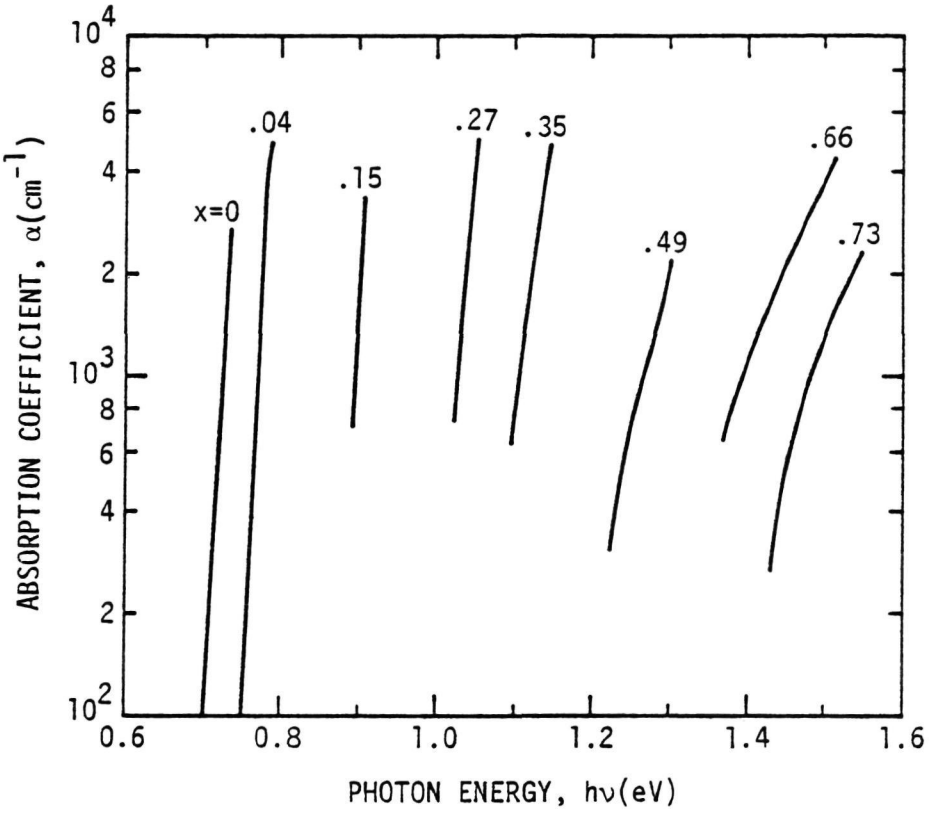

Fig. 3.8 Absorption coefficients of several GaAlSb alloys.

3.3 GaAlSb Ionization Coefficients Measurements

The performance of an avalanche photodiode optical receiver is heavily dependent on the excess shot noise of the APD. The excess shot noise, which essentially is the statistical distribution of the multiplication of the carriers, can be characterized by the carrier secondary ionization rates. The larger the difference between the ionization rates of holes and electrons, the lower will be the excess shot noise (assuming the carriers of the higher ionization rate are photogenerated as primary carriers). Therefore, the ionization coefficients of the electrons and holes in $Ga_{.74}Al_{.26}Sb$ were studied.

The block diagram of the experimental setup for the ionization rate measurement is shown in Fig. 3.9. In order to make accurate measurement, pure electron and pure hole injection into the same junction are essential. The structure of the diode suitable for pure injection is shown in Fig. 3.10. A 0.63μm He-Ne laser is used to inject electrons into the junction. The laser light is strongly absorbed in the first layer and the electron-hole pairs are excited there. The created electrons will then diffuse into the junction and start the multiplication process. A 1.15μm He-Ne laser is used to inject holes into the junction. The first two layers are transparent to 1.15μm radiation which eventually will be absorbed in the third layer. The created holes will diffuse back to the junction and start the multiplication. Subsequently, curves of M_n, electron multiplication and M_p, hole multiplication, vs bias voltage are taken.

The relations between α, the electron ionization coefficient, β, the hole ionization coefficient and M_n, M_p are as follows:

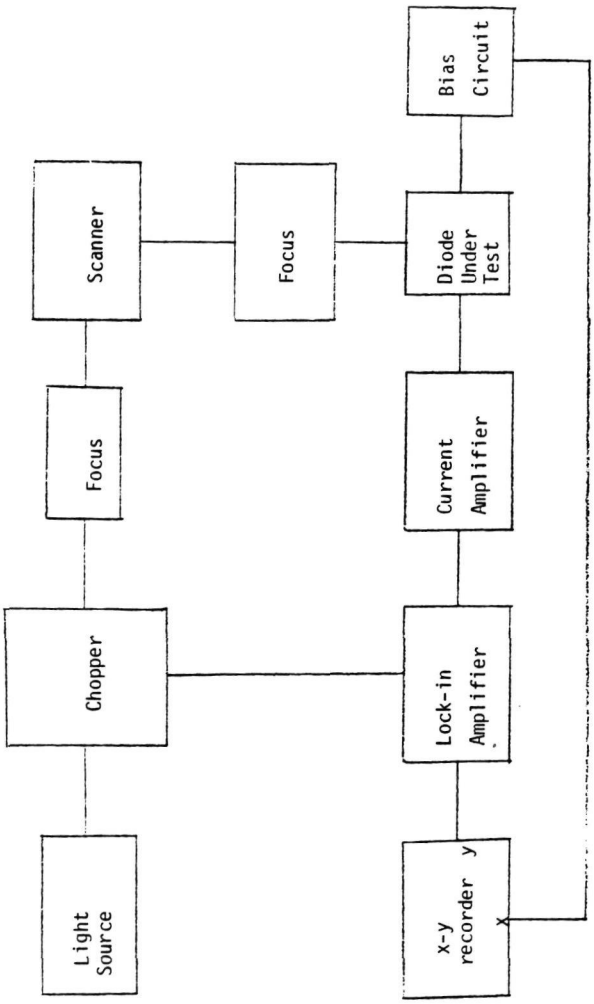

Fig. 3.9 Block Diagram for the Ionization Rate Measurement.

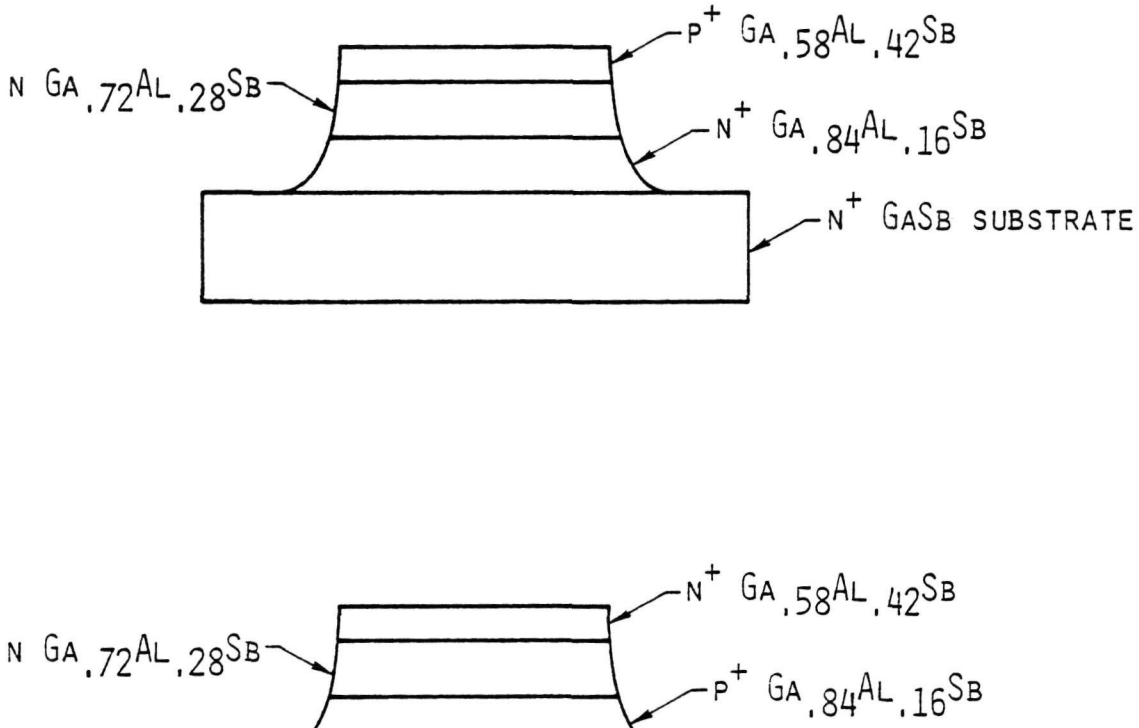

Fig. 3.10 Structure of GaAlSb diodes suitable for pure carrier injection.

$$1 - \frac{1}{M_n} = \int_0^w \alpha \exp\left[- \int_0^x (\alpha-\beta)dx' \right] dx \tag{3.1}$$

$$1 - \frac{1}{M_n} = \int_0^w \beta \exp\left[\int_x^w (\alpha-\beta)\, dx' \right] dx \tag{3.2}$$

$$\ell n \frac{M_n}{M_p} = \int_0^w (\alpha-\beta)\, dx \tag{3.3}$$

where w is the depletion width.

For a one-sided abrupt junction with constant doping on the active layer and under the non-punch through condition, the above equations can be solved with suitable boundary conditions:

$$(E_m) = E_m \left\{ \frac{d(\ell n M_n)}{dV} - \frac{M_n - 1}{M_n} \cdot \frac{d(\ell n M_p)}{dV} \right\} \tag{3.4}$$

$$(E_m) = \frac{E_m}{M_n} \frac{d(\ell n M_p)}{dV} \tag{3.5}$$

where E_m is the maximum electric field and V the bias voltage.

The space charge widening effect can be corrected by best fitting the low bias photocurrent to the following function:

$$J_p = \frac{A}{\cosh\left(\frac{\ell - w}{L}\right)} \tag{3.6}$$

where J_p is the photocurrent, A a constant, L the diffusion length of holes in n-type material, ℓ the length of the active layer, and w the depletion width.

The ionization rates of $Ga_{.74}Al_{.26}Sb$ were measured in five different samples, F1OB1S1-G5, F1OB1S1-G6, F1OB1S1-G7, F1OB1S1-GC1 and F1OB1S1-GC2. The doping of the materials was measured by capacitance-voltage method and found to vary from $7.0x10^{15}cm^{-3}$ to $4x10^{16}cm^{-3}$ covering a wide electric field range for the data. The diodes used in this measurement have all been checked for the junction uniformity. The deduced ionization rates were plotted in Fig. 3.11. A consistent result β/α approximately 2 is found. The numerical constants of α and β are

$$\alpha = 1.04x10^5 \exp\left[-(4.10x10^5/E)^2\right]$$

$$\beta = 1.91x10^5 \exp\left[-(4.12x10^5/E)^2\right]$$

The breakdown voltages of a one-sided abrupt junction uniformly doped n-type diode can be calculated by integrating the above ionization rates. The result is shown in Fig. 3.12. The I-V characteristics measured on a curve tracer agree closely with the calculated breakdown voltage. This self consistency substantiates the good quality of these diodes and the validity of the ionization rate measurement.

The excess noise factor of a $Ga_{.74}Al_{.26}Sb$ avalanche photodiode is estimated to be equal to 0.75 based on the calculations of McIntyre[2] and this ionization coefficients measurement. The excess noise of GaAlSb diode is comparable to GaAsSb 1.06μm APD, and is better than GaAs (where $X_n = 1$). No large anisotropy of ionization rates has been found in any III-V semiconductor. Unlike the case of silicon, the α/β or β/α ratio in all III-V is limited to 5 or less. The III-V avalanche photodiode is still superior to

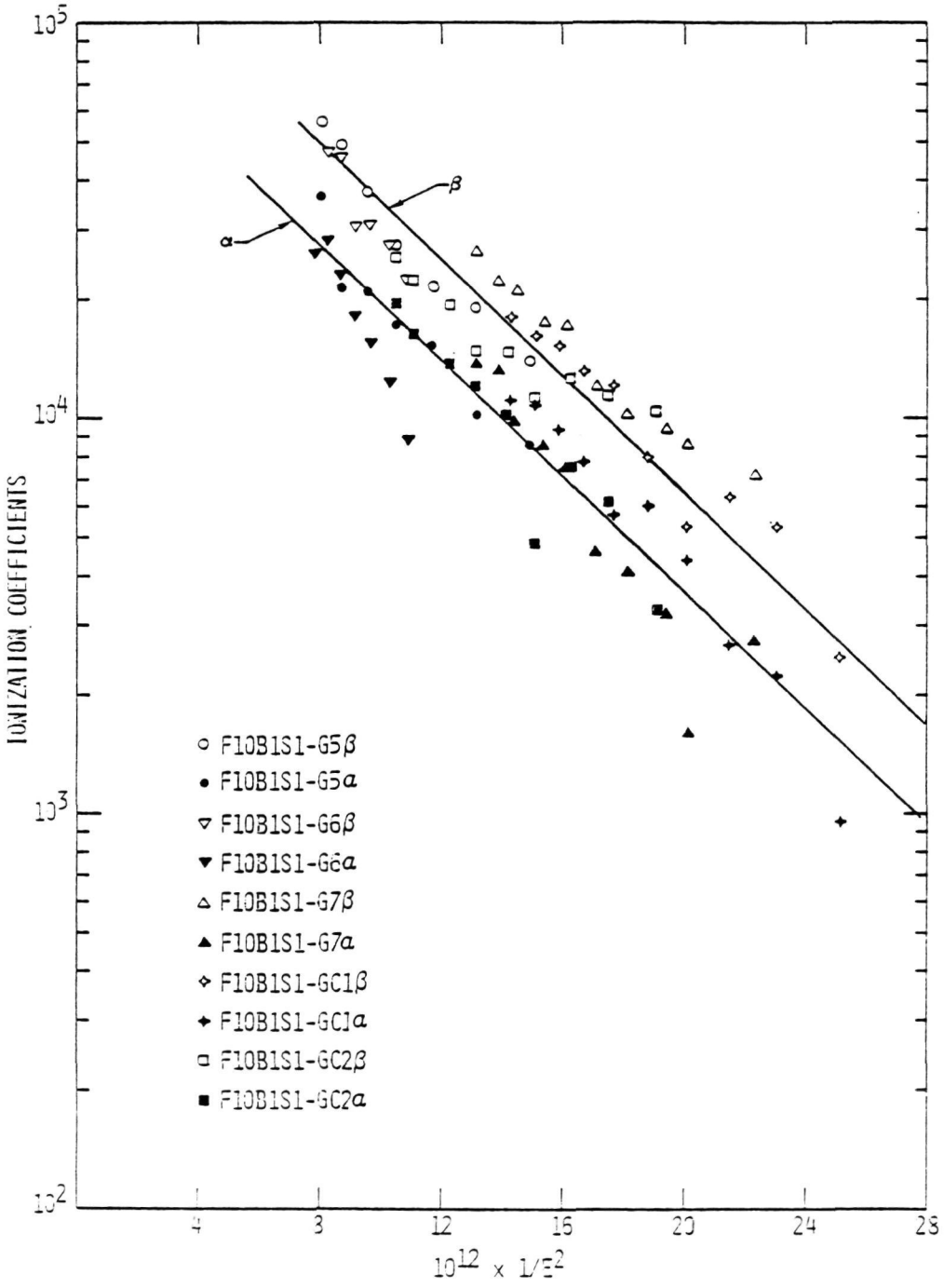

Fig. 3.11 Ionization coefficients for GaAlSb.

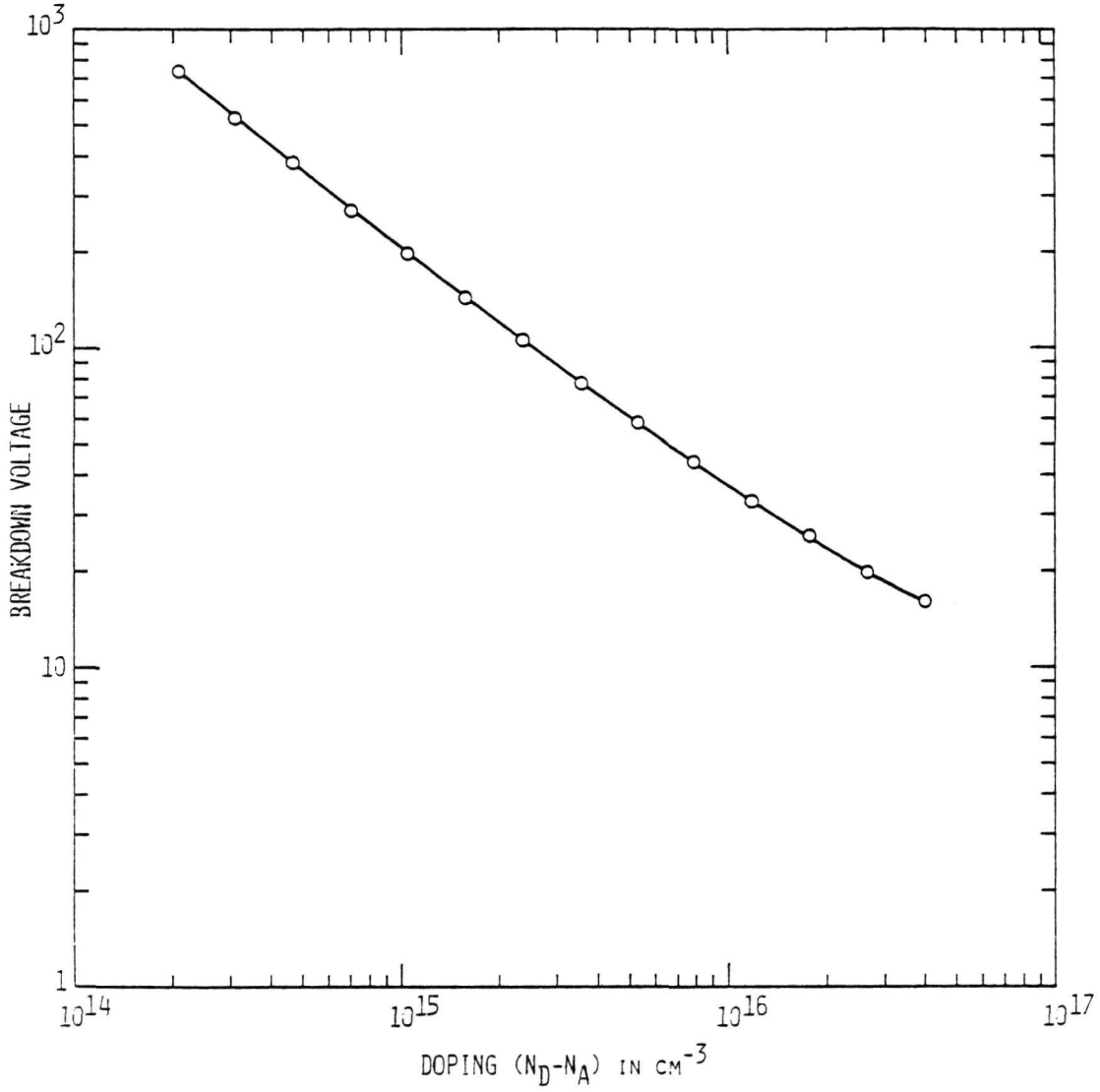

Fig. 3.12 Breakdown voltages of the uniformly doped one-sided abrupt junction n-type $Ga_{.74}Al_{.26}Sb$ diodes at room temperature.

the silicon avalanche photodiode because of their significantly high quantum efficiency due to being direct bandgap materials.

3.4 GaAlSb 1.06μm APD Results

The major goal of this project was to develop a high speed, high quantum efficiency 1.06μm APD's with low dark current suitable for precision rangefinder applications. From the analysis carried out in Section 2, it is obvious that the main parameters for device evaluation are quantum efficiency and risetime. Thus in the design of the diode the depletion region must be at least 3μm thick to absorb greater than 95% the incident radiation. The speed of the photodiode depends on the capacitance of the diode as well as the transit time of the carriers through the diode. Lowering the doping of the active region will increase the depletion region and therefore reduce the capacitance of the diode. Increasing the depletion width, however, increases the carrier transit time. The fastest structure is one in which the RC time constant and transit time are equal. The optimum depletion width is found to be 3-4μm in GaAlSb. Thus, both high speed and high quantum efficiency can be optimized in GaAlSb. This is not the case in indirect gap materials (like Si or Ge) where thicker active regions are necessary for high quantum efficiency. Thus to make high speed detectors indirect gap materials must sacrifice quantum efficiency. Figure 3.13 shows a schematic of the GaAlSb APD.

The noise performance of the device is dependent on the reverse leakage of the device. Figure 3.14 shows the reverse characteristics of a 3 mil GaAlSb. The reverse bias current shown in Fig. 3.14 represent nearly an order of magnitude improvement of the dark current reported in Contract NAS5-22806. This is a result of better doping control described in a previous

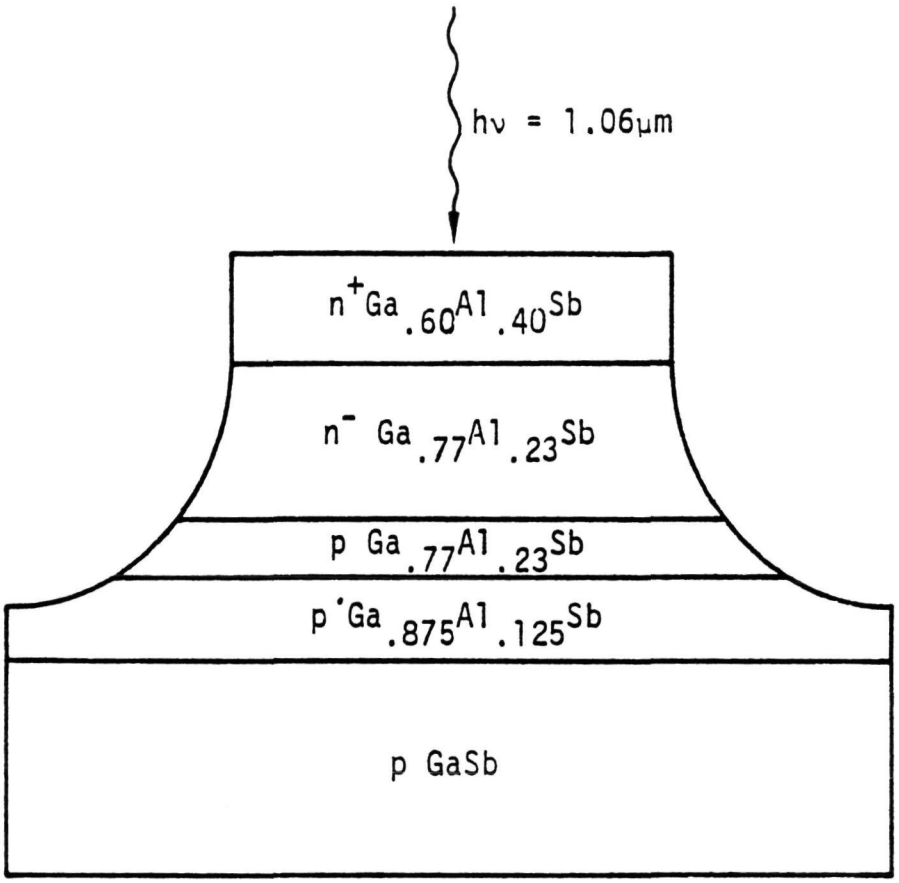

Fig. 3.13 GaAlSb APD structure.

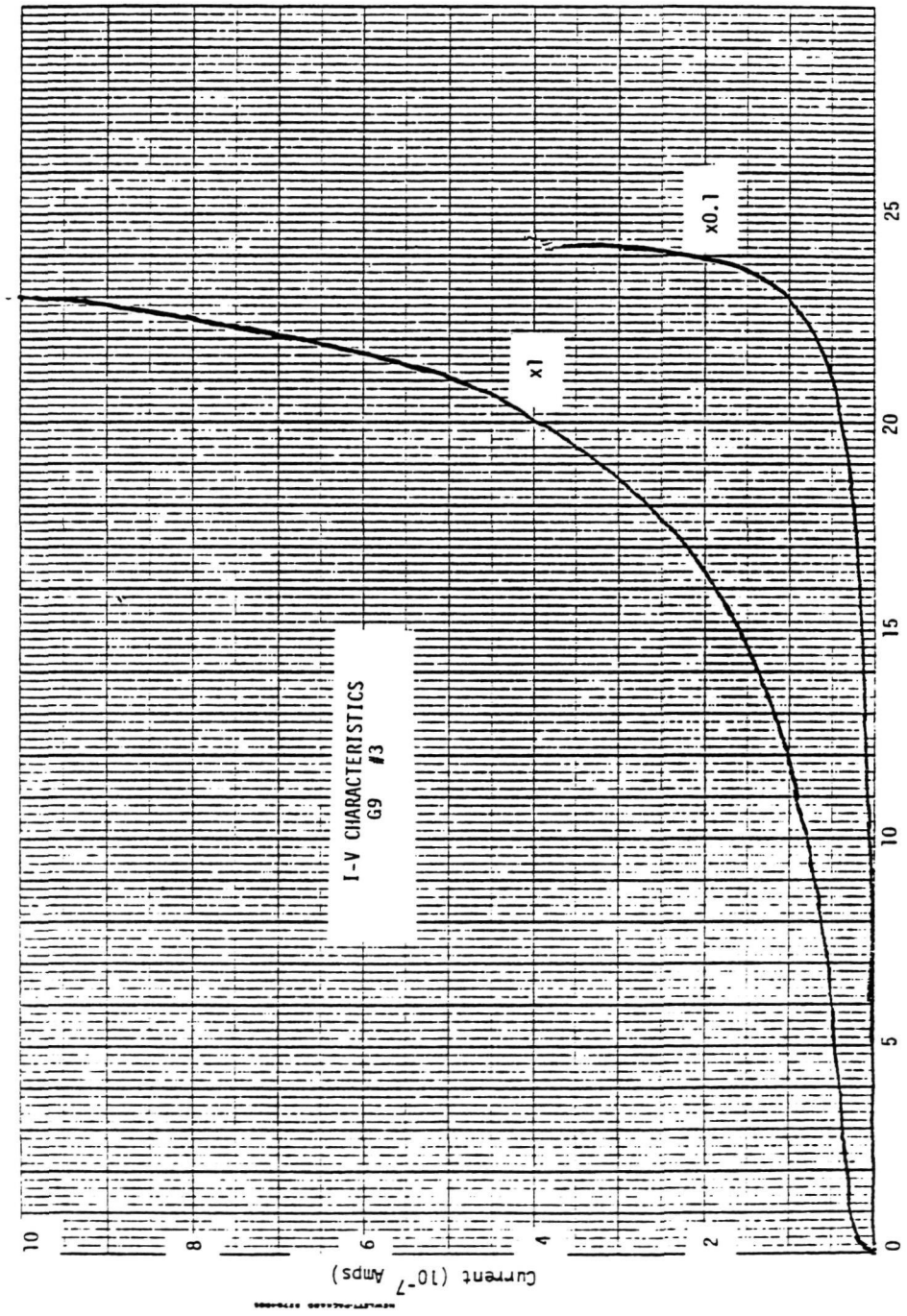

Fig. 3.14 Reverse characteristics of a 1.06μm GaAlSb APD.

section. Further improvement should be possible by reducing surface leakage current by passivation techniques.

Figure 3.15 shows an intensity modulated gain uniformity scan across the area of the detector at gains of 1 and 5. Notice the absence of microplasma gain, hot spots or edge breakdown. The optically active area is the lower circular part of each photo. The upper area is the bonding pad. Gain uniformity across this diode is better than $\pm$ 10%. Figure 3.16 shows a trace of gain vs distance for a GaAlSb APD fabricated under this program. Compare that to Fig. 3.17 which shows a typical GaAsSb APD fabricated under Contract NAS5-22806.

Figure 3.18 shows the photoresponse of a typical GaAlSb detector designed for operation near 1.06μm. This same alloy system can easily be extended to operate anywhere from 1.0μm to 1.8μm.

The microwave avlanche gain, measured again with a 273 MHz repetition rate mode locked Nd:Yag laser, ranged from 20-100 for these devices. Figure 3.19 shows the photorespone vs bias voltage of a typical GaAlSb APD. The upper curve shows the photoresponse to a 273 MHz repetition rate mode locked Nd:Yag. The next curve shows the dark current response. The lower curve shows the photoresponse with the spectrum analyzer tuned away from 273 MHz. Figure 3.20 shows the high speed pulse response of the APD to the mode locked Nd:Yag laser. Figure 3.21 shows a high resolution pulse shape showing a 60ps risetime. This is by far the fastest response time ever reported for a 1.06μm detector. The fall time is equivalently fast indicating that nearly 100% of all photogenerated carriers are absorbed in the high field region. This is the key to achieving high quantum efficiency, ultra high speed APD's.

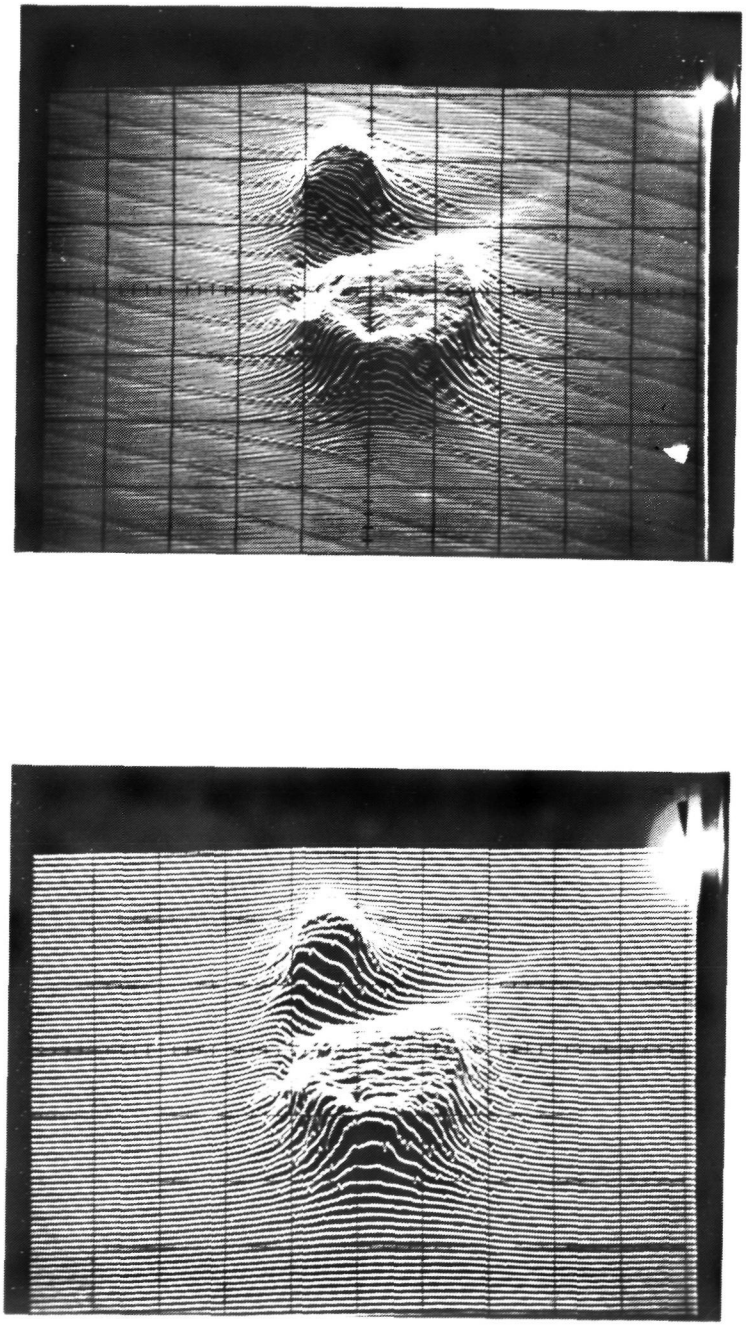

Fig. 3.15 Intensity modulated gain uniformity of a GaAlSb APD. (upper M=1), (lower M=5).

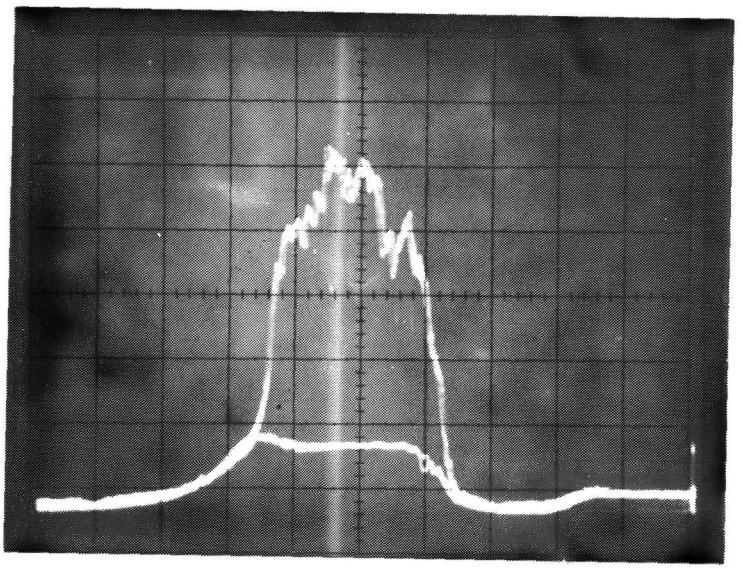

Fig. 3.16 Gain vs. distance across active area of a GaAlSb APD. (M=5)

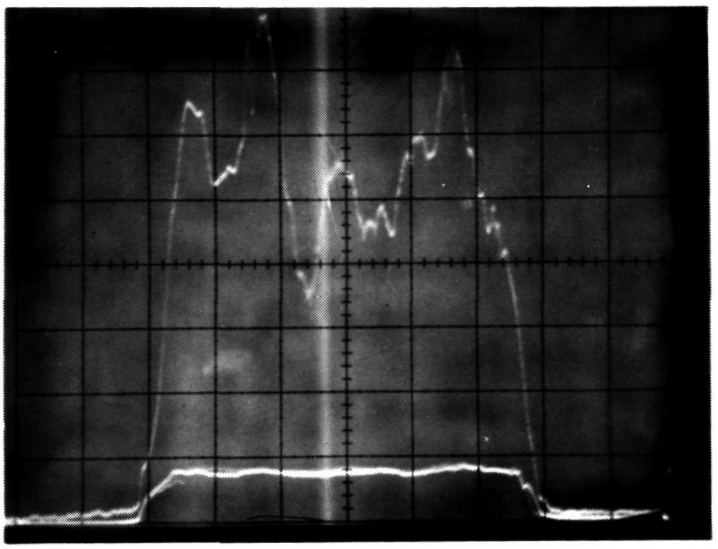

Fig. 3.17 Gain vs. distance across active area of best GaAsSb APD.

Fig. 3.18 Photoresponse of GaAlSb APD grown for 1.06μm applications.

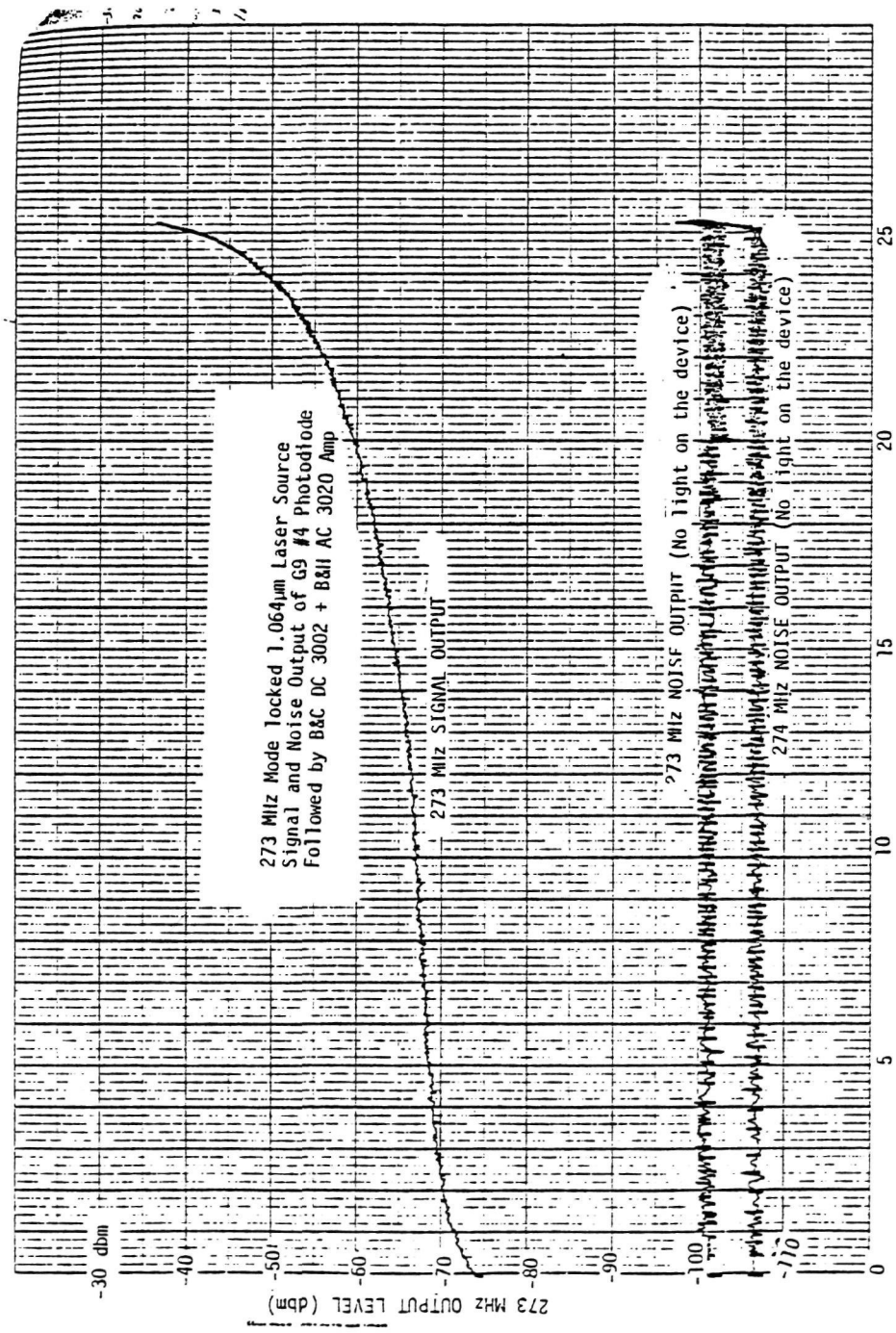

Fig. 3.19 High speed photoresponse versus bias voltage for a GaAlSb APD.

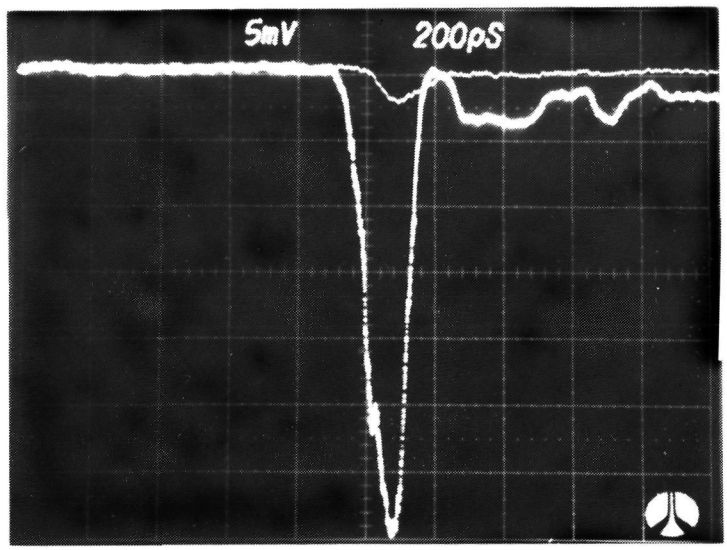

Fig. 3.20 Pulse response to a mode locked Nd:YAG laser. Upper trace M=17, lower trace M=1.

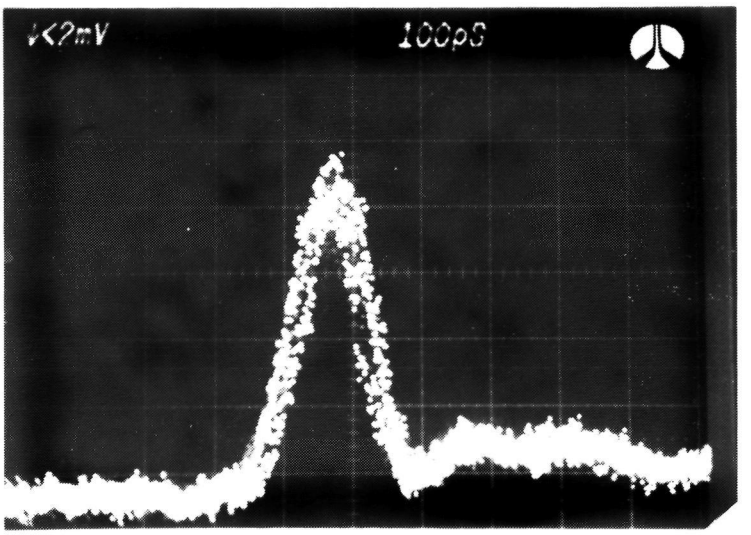

Fig. 3.21 High resolution 1.06μm pulse response.

The complete data sheets supplied with the two 1.06μm APDs delivered under this contract are provided in the Appendix.

3.5 Rangefinder Receiver Analysis

NASA programs in geophysics require precision optical rangefinder technology. In this section, we analyze two approaches to achieve better than 2 cm range resolution at very low (10-100 photons) received photon levels. The analysis of each system will compare the performance of III-V avalanche photodiode technology developed at the Science Center, in part with NASA support, with existing photomultiplier tube technology. The systems are required to have pulse widths of less than 750ps in order to detect the transit time differences of the two colors resulting from dispersion in the atmosphere. This delay is estimated to be 1-3ns depending on the transmitted angle through the atmosphere. A single electronic amplifier chain is used to eliminate time drifts between the channels and simplify receiver calibration. The two systems that are analyzed are:

1. Single Color System - In this system the performance of a 1.06μm laser-1.06μm APD receiver will be compared with a 1.06μm doubled laser-.53μm PMT receiver.
2. Two Color System - In this system the performance of an APD rangefinder based on 1.06μm and its 2nd harmonic (.53μm) will be compared with a 2nd and 3rd (.35μm) harmonic of 1.06μm using photomultiplier tubes as the detector.

In both these systems, the source will be a 1.06μm Nd:Yag laser. The following assumptions are made concerning 2nd and 3rd harmonic generation.

For 2nd harmonic generation 67% of the incident 1.06μm energy is converted to .53μm. The resulting photon generation efficiency, based on the Nd:Yag laser generating 1.06μm photons at 100% efficiency is 33% at 1.06μm and 33% at .53μm. This means that relative to a 1.06μm single color system there are only 33% as many 1.06μm photons and 33% as many .53μm photons. For 2nd and 3rd harmonic generation we assume that the power is equally divided among the three wavelengths resulting in photon conversion efficiencies of 33% for 1.06μm, 16% for .53μm and 11% for .35μm.

For the PMT systems we assume that the quantum efficiency is 20% and that no excess multiplication noise is generated (i.e. $X_n = 0$). A risetime of 100ps is assumed and represents a risetime that is twice as fast as has been demonstrated with this technology. The time jitter due to signal shot noise is thus described by

$$\Delta T_{rms} = \frac{T_{PR}}{\sqrt{\eta N_p}} \tag{2.18}$$

where T_{PR} is the risetime

η is the quantum efficiency

N_p is the number of incident photons.

For the APD analysis we will use device performance parameters demonstrated as part of our present NASA contract work. The integrated hybrid receiver performance is based on previous NASA[4] and AFAL[5] contract work using very high speed Science Center FET devices. The assumptions are: quantum efficiency of greater than 90%, a multipication gain of 30 and an excess noise factor of .75 ($X_n = .75$).

The major elements of the APD technology that will be exploited to show the system performance advantage of APD/hybrid integrated GaAs FET electronics over PMT technology are:

1. higher speed of APD technology - risetimes of less than 25ps have been demonstrated for III-V APDs. The APD/GaAs FET electronics can provide a 50ps risetime for the NASA rangefinder application. Since the time jitter is proportional to the voltage noise divided by the waveform slope decreasing the risetime reduces the time jitter.
2. higher quantum efficiency of APD will improve performance by reducing the number of received photons required to achieve a given level of performance.

The time jitter for the APD receiver can be written as

$$\Delta T_{rms} = \frac{T_{PR}}{\sqrt{\eta N_p}} \quad M^{X_n/2} \tag{3.8}$$

when the receiver is signal shot noise limited and

$$\Delta T_{rms} = T_{PR}\left(\frac{4kT}{R_F}\,\Delta f\right)^{1/2}/q\ N_p M\ \ 2\pi\Delta f \tag{3.9}$$

when the receiver is Johnson noise limited.

The receiver proposed here will have an impulse response pulsewidth of less than 500ps in order to clearly distinguish the .53μm and 1.06μm pulses that arrive at the receiver separated by 1-3ns. The design configuration for the two color system is shown schematically in Fig. 3.22 Conceptually, this

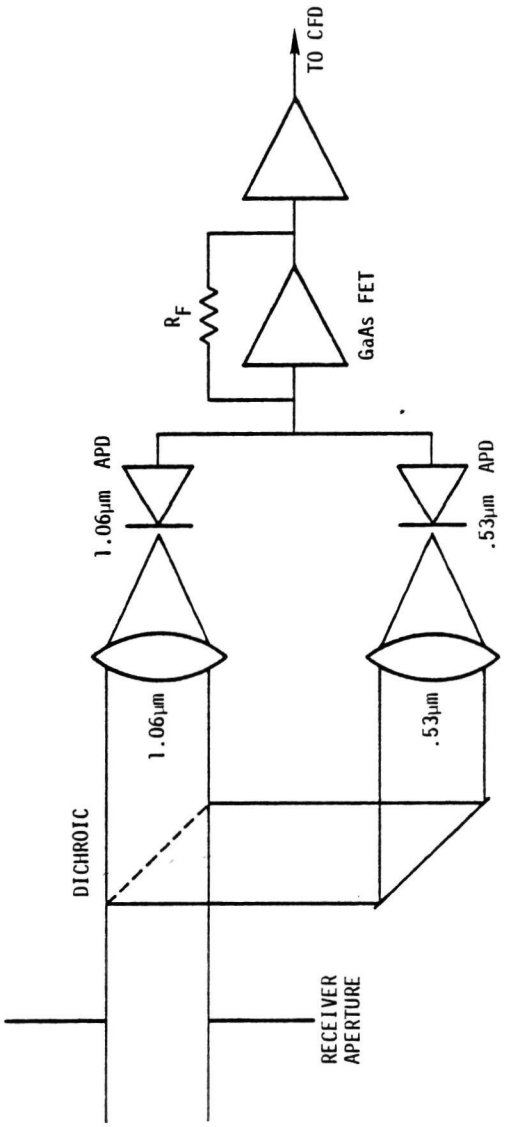

Fig. 3.22 Schematic of two color receiver.

design is similar to the 400 MB/s receiver built for NASA under previous contract support.[4] The internal element values have been changed to meet the faster response times required in the rangefinder application. Significant improvements in Science Center GaAs FET devices have also been incorporated. The use of APDs with significant gain also improves performance over previous receiver work.[4,5]

3.5.1 One Color Receiver

In this case, we are comparing a frequency doubled PMT receiver with a 1.06μm APD receiver. In order to compare performance based on the same 1.06μm transmitter we define the quantity

$$\eta_{net} = \eta_{photon}\eta_{device} \qquad (3.10$$

where η_{photon} is the photon conversion efficiency and η_{device} internal quantum efficiency. Thus, when we plot out time jitter vs number of photons we are comparing performance based on an equal number of photons generated at the source, i.e. $N_p = A\ E_T$

where P_T is the transmitter pulse energy

$A\ E_T$ is a constant, the same for both cases.

For the One Color receiver:

APD: η_{net} (1.06μm) = 90% (100% x 90%)

PMT: η_{net} (.53μm) = 7% (33% x 20%)

The performance comparison is shown in Fig. 3.23 The APD receiver shows superior performance for N_p >15 primarily as a result of the faster risetime capability and higher quantum efficiency. For N_p >10 both systems can meet the time jitter maximum of 100ps (2cm).

3.5.2 Two Color Receiver

For the two color receiver the net efficiencies are:

APD: η_{net} (1.06μm) = 30% (33% x 90%)

η_{net} (.53μm) = 30% (33% x 90%)

PMT: η_{net} (.53μm) = 3% (16% x 20%)

η_{net} (.35μm) = 2% (11% x 20%)

In this APD receiver the R_f is slightly reduced to compensate for increase in input capacitance caused by the addition of the second APD. The performance comparison is shown in Fig. 3.24 The superior performance of the APD receiver is now clearly evident. The APD will meet the 100ps maximum jitter for N_p >10 photons, the PMT system requires N_p >25 photon. If a more stringent maximum time jitter of 50ps is required, the APD receiver can meet the requirement when N_p >20 photons while the PMT system requires N_p > 100 photons. In terms of transmitted power from the spacecraft, equivalent performance can be obtained with the III-V APD two color system using 7 dB less transmitted power. Over the range of 50ps < t_{rms} < 100ps the advantage of the APD receiver over a PMT receiver based on the number of

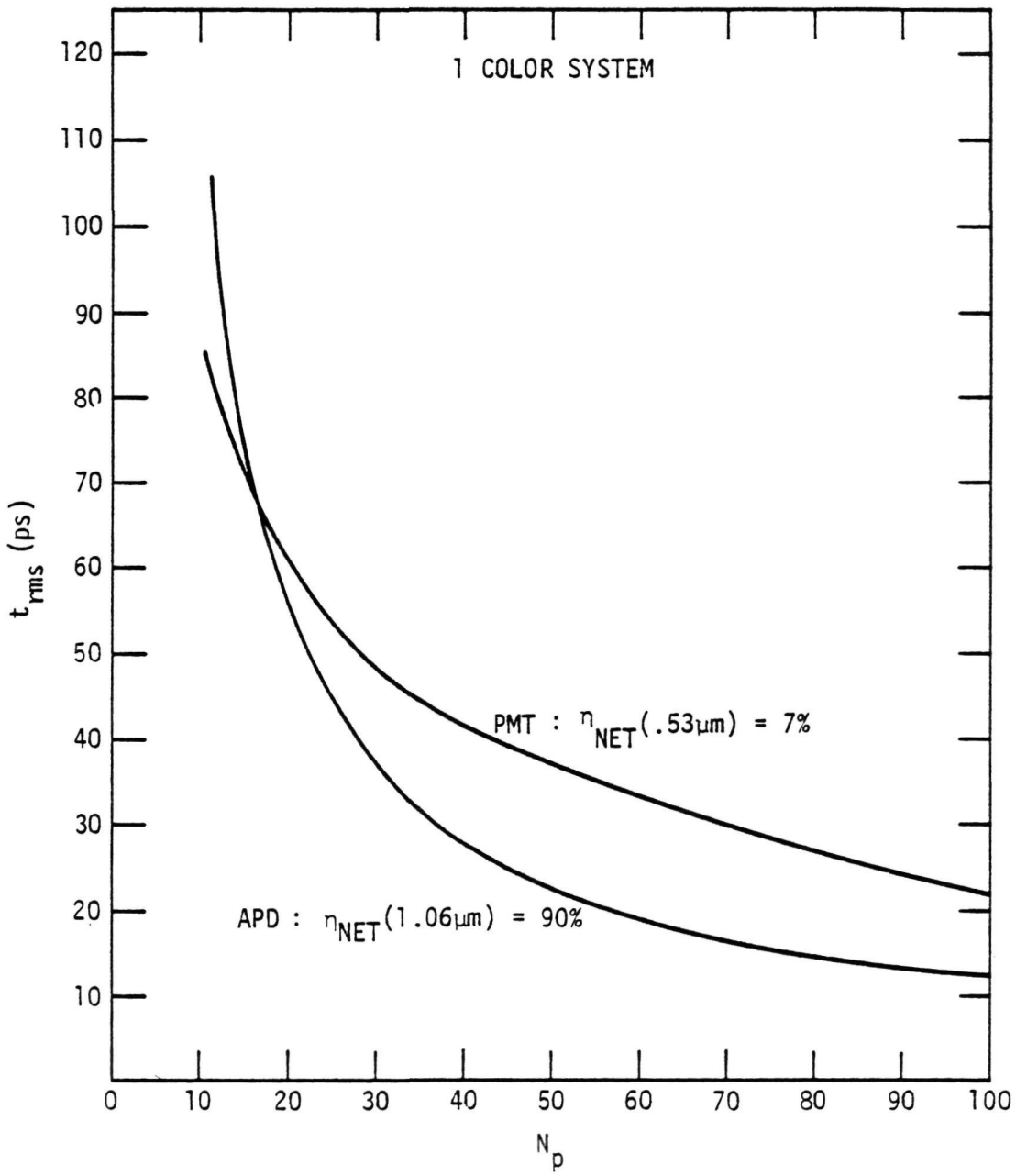

Fig. 3.23 Performance comparison of an APD and PMT one color rangefinder receiver.

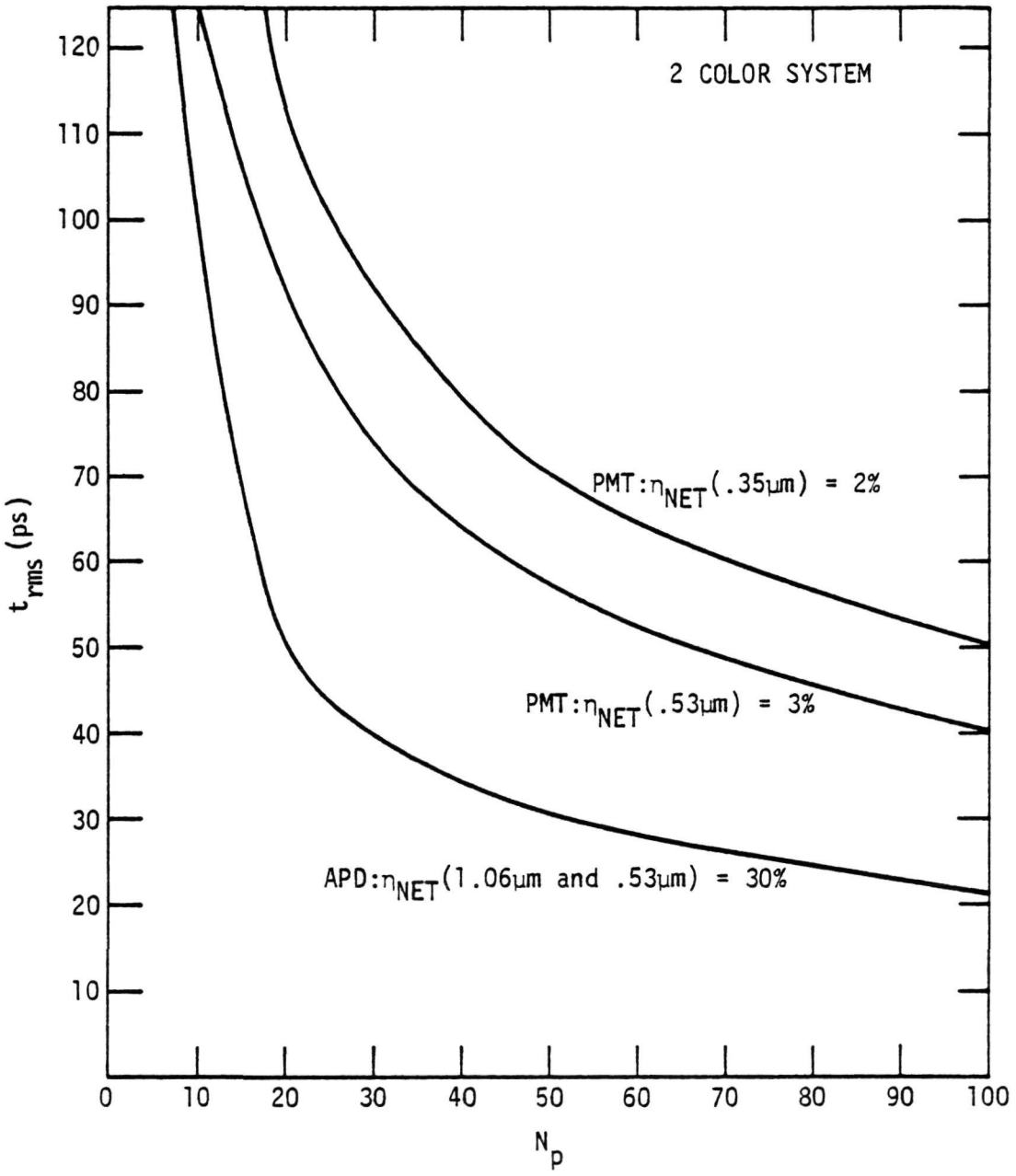

Fig. 3.24 Performance comparison of an APD and PMT two color rangefinder receiver.

photons at the receiver in the baseline system or equivalently on transmitted power from the 1.06μm source is 4 to 7 dB and this advantage increases as the allowed time jitter is reduced.

The vastly superior APD receiver performance compared to a PMT receiver in a two color scenario is a result of:

1. faster risetime
2. higher quantum efficiency
3. the use of less energetic photons

(i.e. 1.06μm and .53μm compared to .53μm and .35μm)

Recall that it takes three 1.06μm photons to make one .35μm photon, yet system performance depends only on the number, not the energy, of received photons.

The inherent time delay in each APD does not degrade performance since total transit time is less than 10ps and internal time jitter is less than 2ps for $N_p > 10$ photons. The inherent jitter remains a potential problem for PMT receivers.

In summary, a III-V APD receiver offers 4-7 dB better performance compared to a PMT receiver when used in a two color rangefinder scenario. This results from faster risetime, higher quantum efficiency and effective use of longer wavelength photons. PMT based systems theoretically and practically cannot compete with III-V APDs in these three areas.

4.0 CONCLUSIONS AND RECOMMENDATONS

The major conclusions of this work are: (1) that high performance 1.06μm avalanche photodetectors can be fabricated in the GaAlSb system. These devices have high quantum efficiency (90%), high speed (risetime < 60ps) and low leakage currents (<50na). The dark current represents more than an order of magnitude reduction compared to previously reported results. The high speed avalanche gain of these devices is between 20 and 50. The area uniformity is better than ± 10%. (2) GaAlAs APDs at 0.53μm have even faster speed (risetimes ~ 35ps), lower dark currents (≤10pa) and high speed gains of 100-200. (3) Optical rangefinders based on measured III-V APD performance parameters have far superior performance when compared to even ideal PMTs in either a one color or two color rangefinder system.

For a one color system, a factor of two lower time jitter can be achieved with identical transmitted power. While for the two color receiver nearly an order of magnitude more transmitted power is required for the PMT receiver system to reach a 30ps time jitter level. The superiority of the APD based two color receiver is significant and exists of the entire range of desired time jitters (<100ps) and received power levels.

We strongly recommend that the III-V APD technology be fully exploited by developing hybrid integrated 0.53μm and 1.06μm optical receivers that will meet NASA rangefinder requirements. We are firmly convinced that other technologies cannot meet the performance levels (speed and quantum efficiencies) demonstrated by the III-V APDs developed under this contract.

REFERENCES

1. S.S. Anderson, F.W. Scholl and J.S. Harris, Inst. Phys. Conf. Sci. No. 33b, p. 346 (1977), Inst. of Phys, Bristol and London.

2. R.J. McIntyre, IEEE Trans. of Elect. Dev. 19, 703 (1972).

3. "Long Life Photomultipler Tubes," Technical Report AFAL-TR-76-148, April 1977.

4. "1.06μm Avalanche Photodiode Detectors with Integrated Circuit Preamplifiers," Final Technical Report for Contract NAS5-23333, December 1975.

5. "1.06μm Avalanche Photodiode Detector," Technical Report AFAL-TR-76-74, May 1976.

APPENDIX A.1

Delivered 0.53μm APD Performance Results

DATA SHEET

B1 S4 0.53μm Photodiode Date: 9/1/77

Device area = equivalent to 2.5 mils diameter dot. (figure eight shape diode).

Depletion width = 2μm.

N_D (doping) = $5x10^{15}/cm^3$.

Capacitance = 0.15 pf @ 40V.

$V_{breakdown}$ = 83V.

Spectral response 500nm - 850nm.

$T_{risetime}$ < 50psec (calculated value 35psec) (risetime is laser pulse limited)

Maximum current allowed ~300μA.

Apply negative bias to the microdot connector.

When operating near breakdown voltage, be very careful that the mode locked pulses are very stable. A sudden large pulse may destroy the device.

A current limiting power supply is absolutely essential.

NAS5-23862-SC5094.25FPR Fig. A.1

BlS4 0.53µm Photodiode

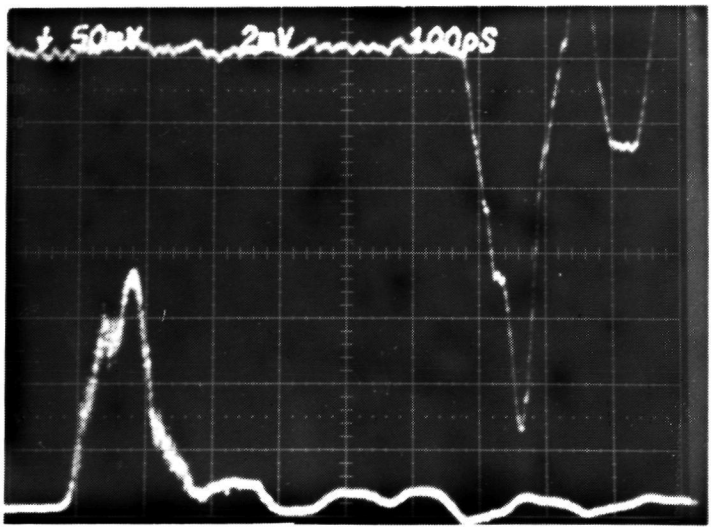

0.53µ pulse response

1.06µpulse response

1.06µm photodiode

Fig. A.1 Nd:YAG mode locked pulse response. Upper curve is the 0.53µm pulse response from 0.53µm detector. Lower curve is the 1.06µm pulse response from 1.06µm detector. Horizontal scale is 100 psec/div.

DATA SHEET

0.53μm High Speed Photodiode Date: 1/10/78

t_r < 50ps

M (gain at low light level) 100

Spectral Response: 500nm to 850nm.

Maximum Reverse Voltage: 54V

Maximum Reverse Current: 400μA

Operating Voltage: 50V

I-V Characteristics: See attached data sheet.

Pulse Response: See attached Photo.

Diode Response vs Reverse Bias: See attached data sheet.

Note: Connect negative bias to the microdot connector.

Connect sampler head or current amplifier to the OSM Connector.

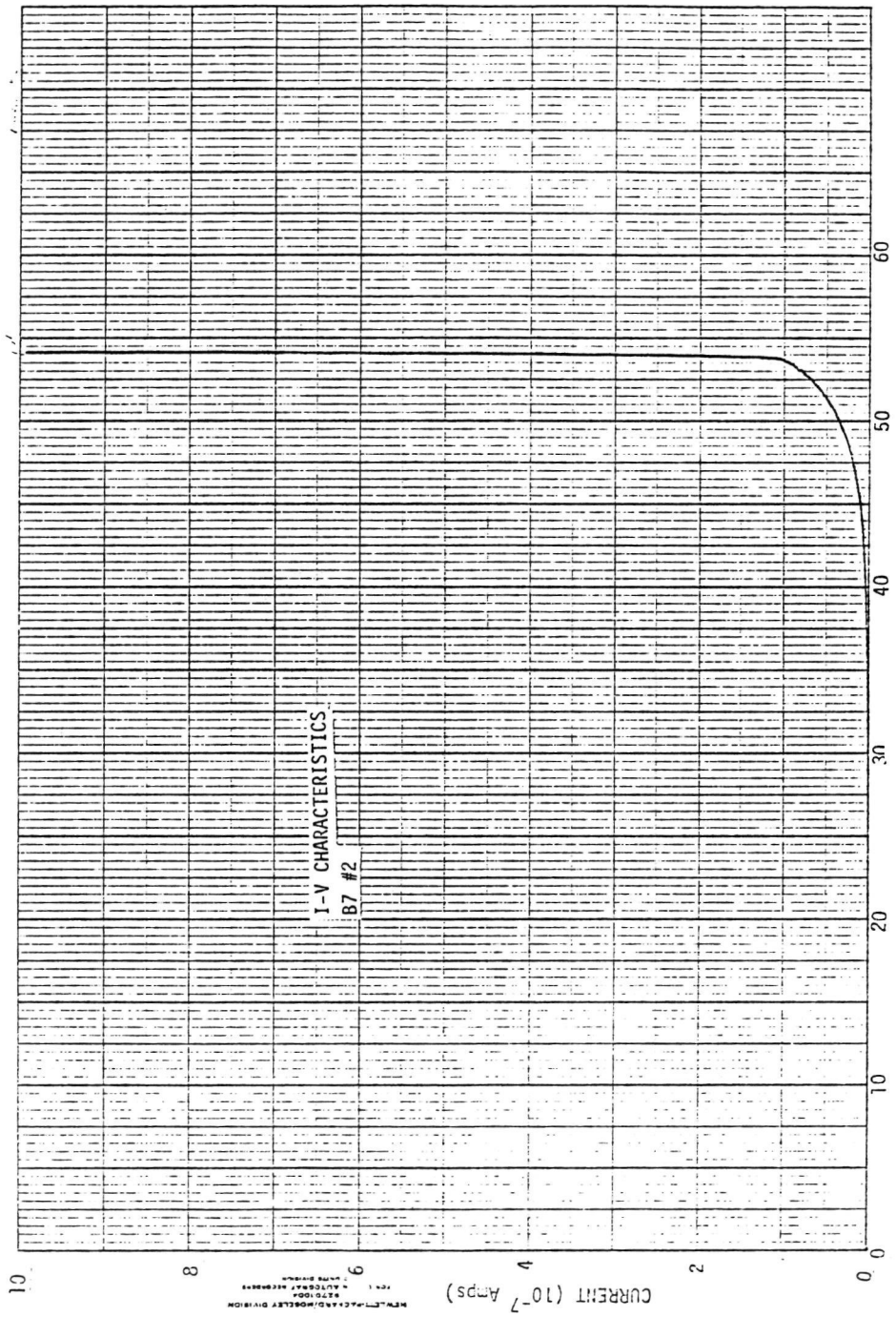
I-V CHARACTERISTICS
B7 #2
CURRENT (10^{-7} Amps)
REVERSE BIAS VOLTAGE (Volts)
0
2
4
6
8
10
0
10
20
30
40
50
60

Fig. A.2

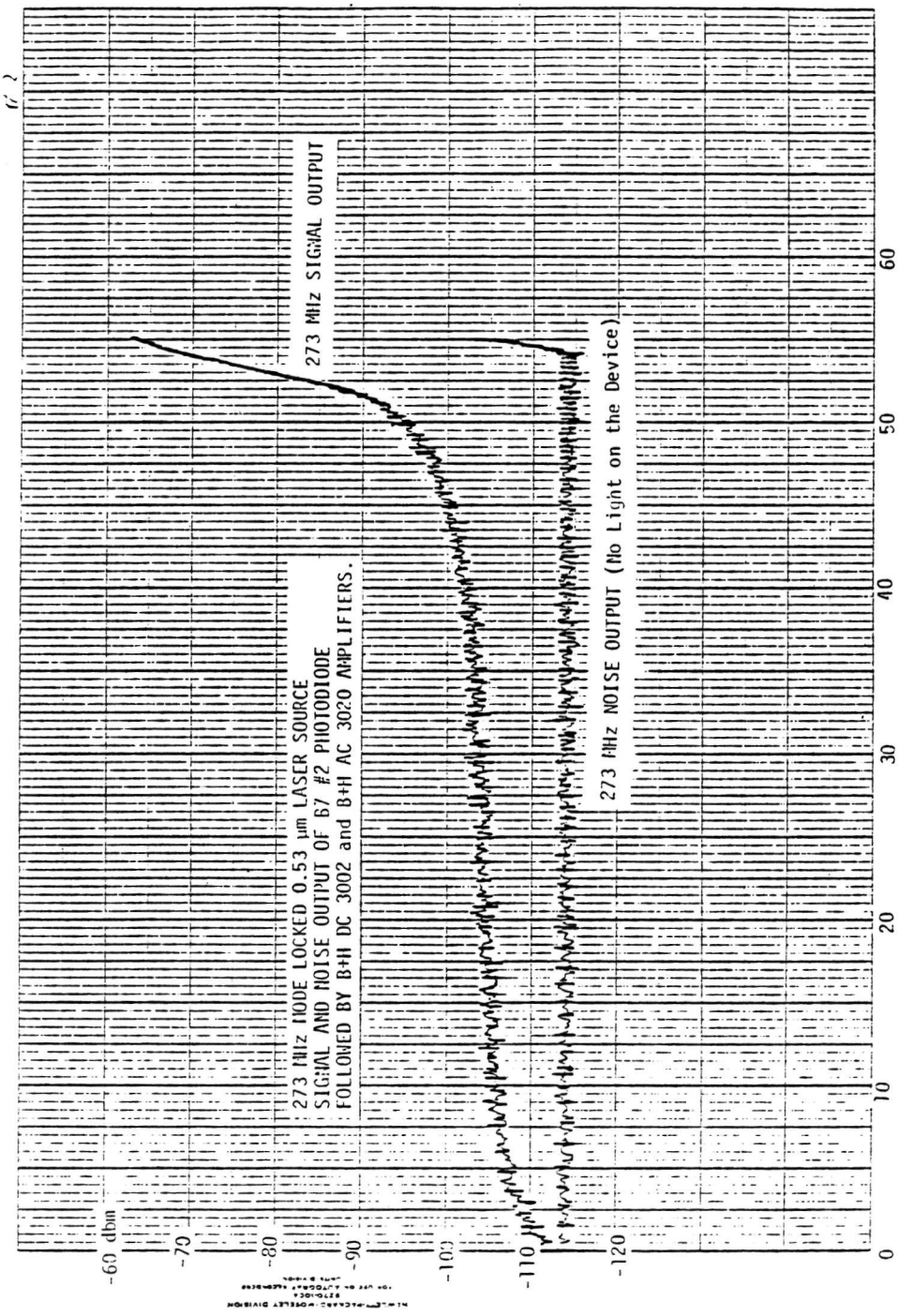
273 MHz SIGNAL OUTPUT
273 MHz NOISE OUTPUT (No Light on the Device)
273 MHz MODE LOCKED 0.53 μm LASER SOURCE
SIGNAL AND NOISE OUTPUT OF B7 #2 PHOTODIODE
FOLLOWED BY B+H DC 3002 and B+H AC 3020 AMPLIFIERS.
273 MHz OUTPUT LEVEL (dbm)
-60 dbm
-70
-80
-90
-100
-110
-120
0
10
20
30
40
50
60
REVERSE BIAS VOLTAGE (Volts)

Fig. A.3

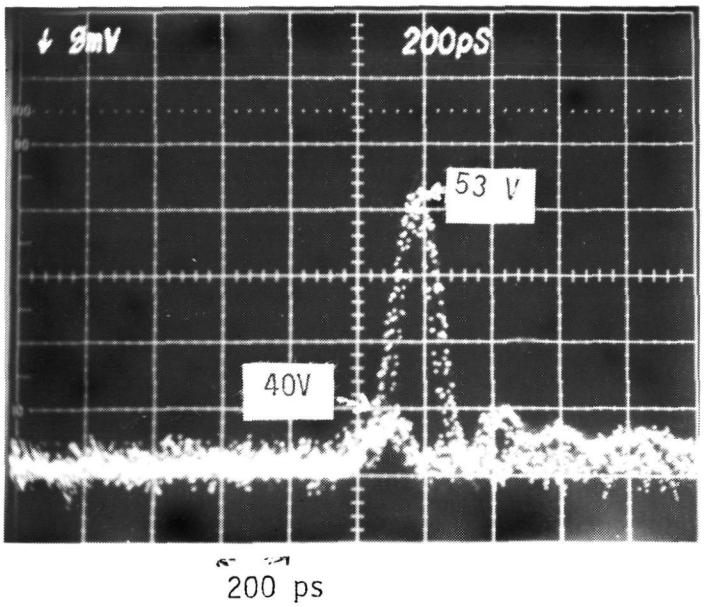

Fig. A.4 0.53μm mode locked laser pulse response. Upper curve 53V, 5 mV/div (vertical), 200 ps/div (horizontal); lower curve 40V, 2 mV/div (vertical), 200 ps/div (horizontal).

NOTE: IT IS IMPERATIVE TO USE A CURRENT-PROTECTED POWER SUPPLY WITH THESE DEVICES!

The power supply for use with these high speed GaAs photodiodes must be current protected or it is simply a matter of time before some "minor" mistake (supply voltage spike, someone inadvertently leaving out a beam attenuator, etc.), annihilating the diode. This can be avoided by taking care to use at least a simple current limiter on the supply.

A very simple current-limited battery powered 40 volt supply suitable for use with these detectors is shown in Fig. 1.

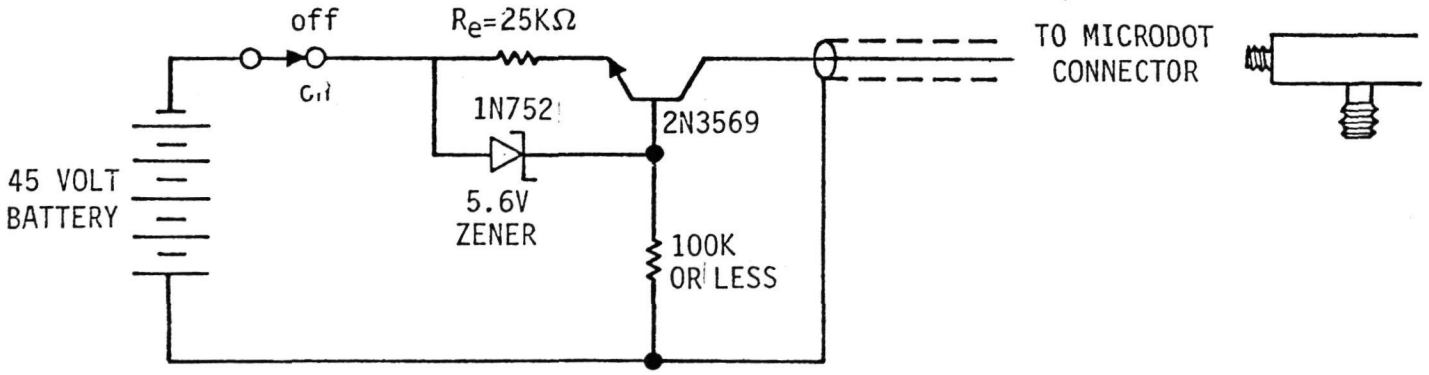

FIG. A.5 Battery-Powered 40 volt supply

The maximum average power dissipation in the photodiodes should be held to about 10mW. It is suggested that power levels be kept somewhat lower than these maximum values for longest device life. Usually, in monitor applications with the device operating directly into a 50Ω sampling oscilloscope head, a 200μA average modelocked laser signal current is sufficient for a good display and the device power is (for a -40 volt bias) $P_D = P_{LIGHT} = V_B I_P = 8$ mW. A current-protected supply using a standard lab supply (0 to -100 volt or whatever) is shown in Fig. 2.

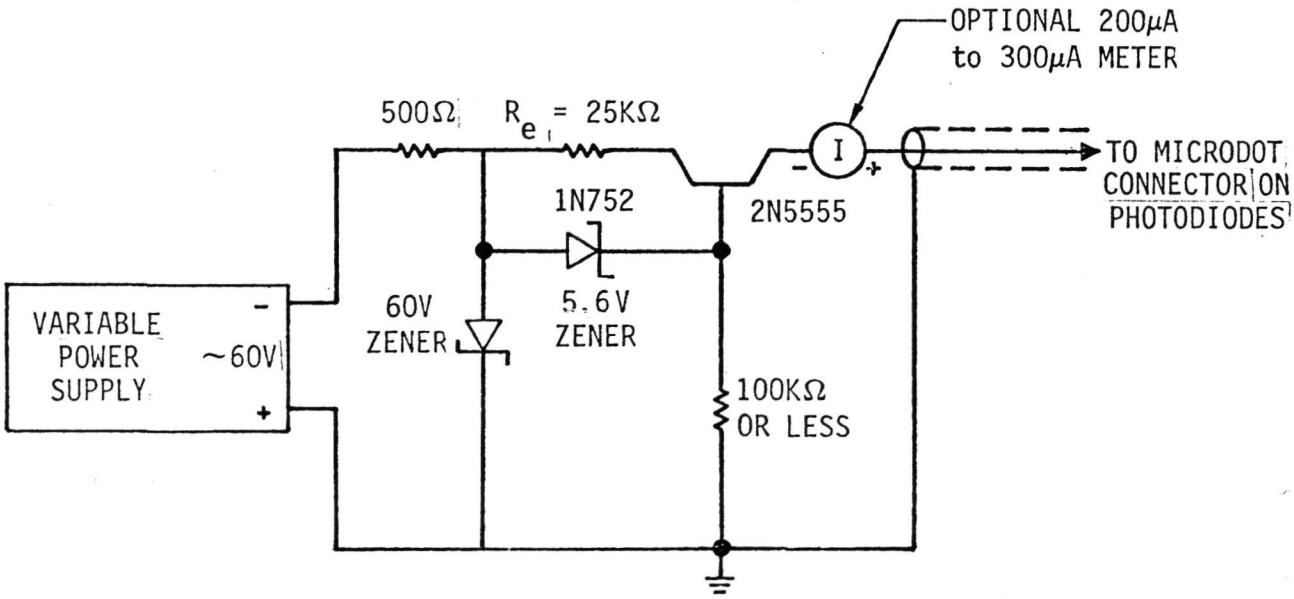

Fig. A.6 Simple current limiter for a lab supply for photodiode.

The input zener diode protects the photodetector from high-voltage spikes on the supply (frequently associated with turn-on or turn-off of the supply). The monitor current meter is very handy in setting "finding the device" with the beam by first defocussing the lens a bit to find the signal, etc. Note that the output voltage is about 5 volts less than the input supply voltage. The output voltage can be monitored essentially as the voltage across the 100KΩ resistors in Fig. 1 and 2 without the current through the voltmeter contributing to the limit current.

APPENDIX A.2

Delivered 1.06μm APD Performance Results

DATA SHEET

1.064μm High Speed Photodiode G9 #3 Date: 1/31/78

$t_r < 50ps$

M (gain at low level) 15

Quantum Efficiency: 88% @ 12V. See attached data sheet.

Maximum Reverse Voltage: 24V

Maximum Reverse Current: 400μA

I-V Characteristics: See attached data sheet.

Pulse Response: See attached photo.

Diode Response vs Reverse Bias (273 MHz): See attached data sheet.

Note: Connect negative bias to the microdot connector.

Connect sampler head or current amplifier to the OSM connector.

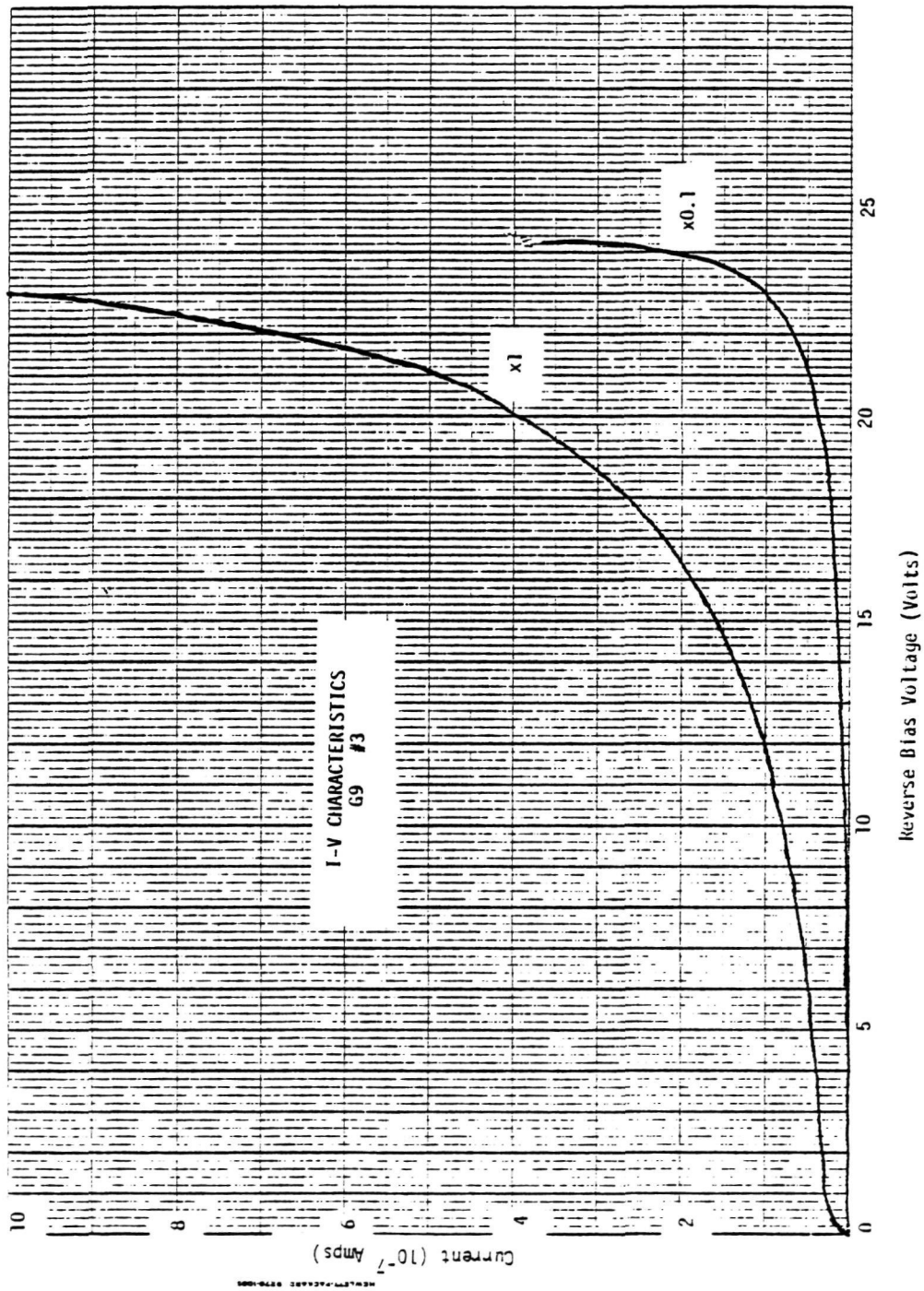
I-V CHARACTERISTICS
G9 #3
x1
x0.1
Current (10^{-7} Amps)
Reverse Bias Voltage (Volts)
0
2
4
6
8
10
5
10
15
20
25

Fig. A.7

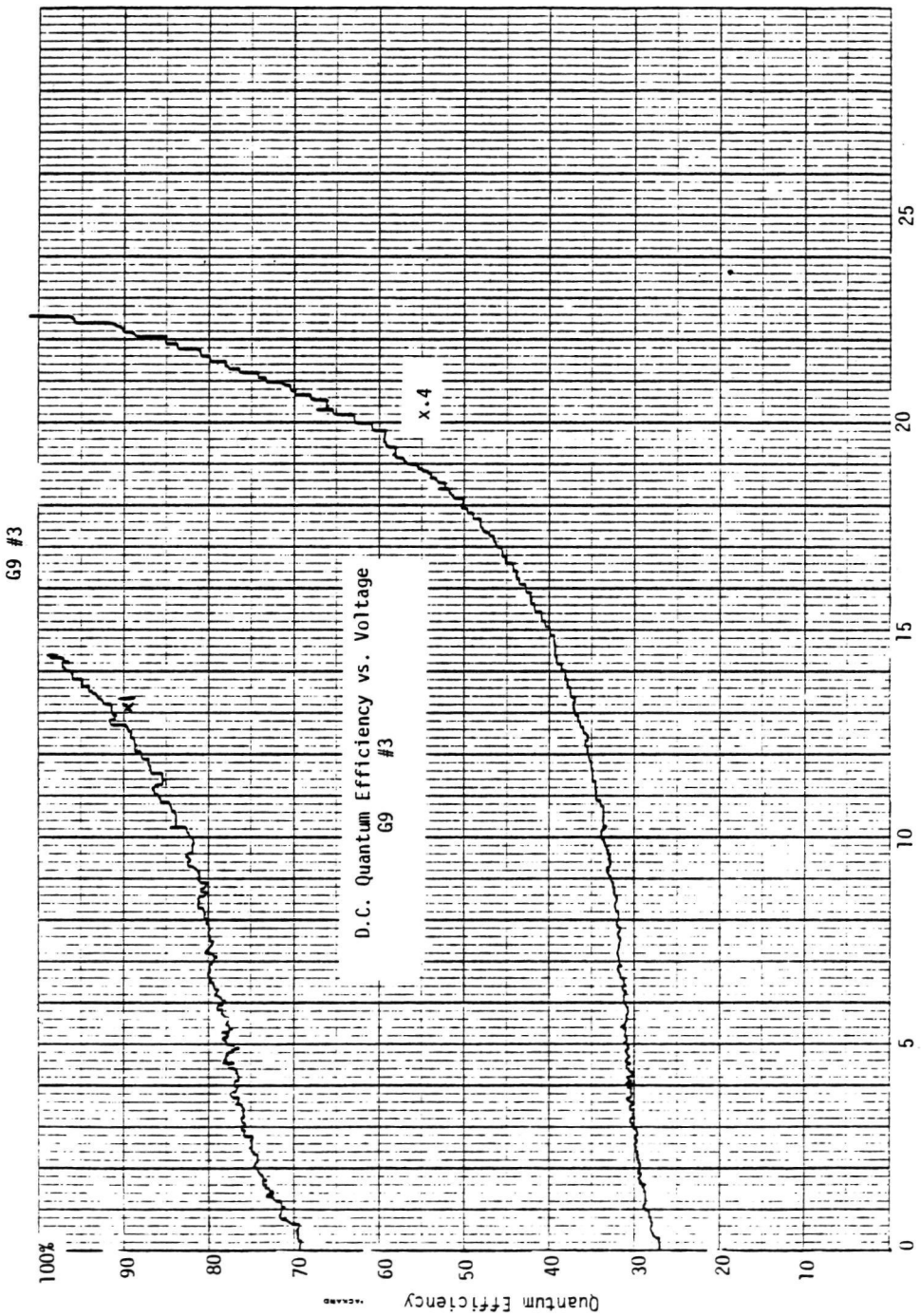
G9 #3
D.C. Quantum Efficiency vs. Voltage
G9 #3
x.4
x1
Quantum Efficiency
100%
90
80
70
60
50
40
30
20
10
0
5
10
15
20
25
Reverse Bias Voltage (Volts)

Fig. A.8

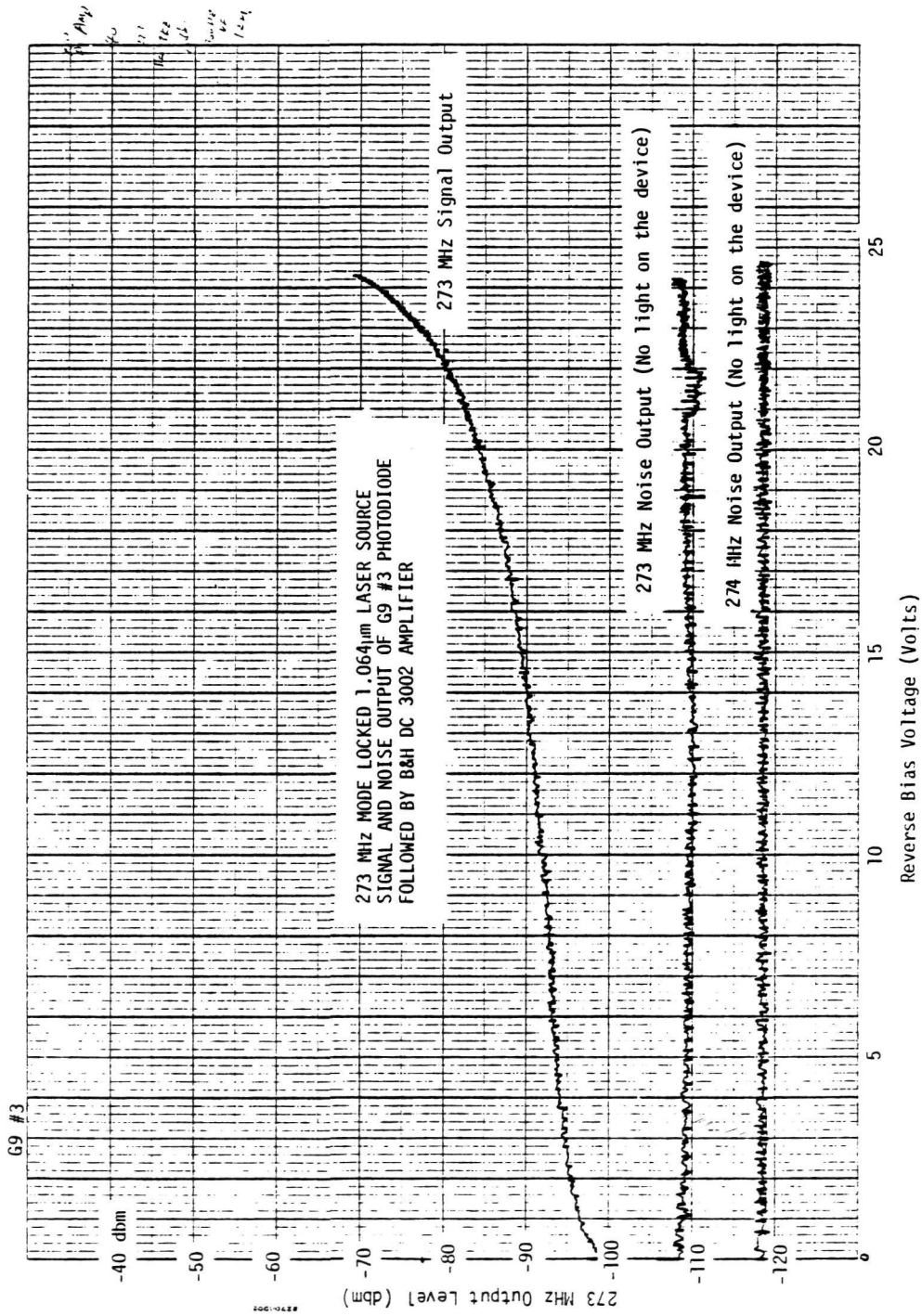
G9 #3
273 MHz MODE LOCKED 1.064μm LASER SOURCE
SIGNAL AND NOISE OUTPUT OF G9 #3 PHOTODIODE
FOLLOWED BY B&H DC 3002 AMPLIFIER
273 MHz Signal Output
273 MHz Noise Output (No light on the device)
274 MHz Noise Output (No light on the device)
273 MHz Output Level (dbm)
-40 dbm
-50
-60
-70
-80
-90
-100
-110
-120
0
5
10
15
20
25
Reverse Bias Voltage (Volts)

Fig. A.9

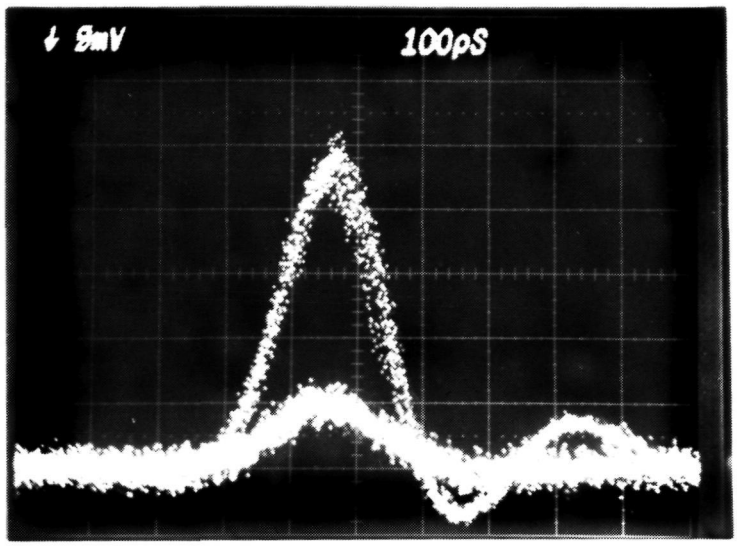

Fig. A.10 1.064μm mode locked laser pulse response for G9#3 diode. Upper curve 24V, 5 mV/div (vertical), 100 ps/div (horizontal); lower curve 5V, 2 mV/div (vertical), 100 ps/div (horizontal).

SC5094.25FPR

DATA SHEET

1.064μm High Speed Photodiode G9 #4 Date: 1/31/78

$t_r < 50ps$

M (gain at low light level): 30

Quantum Efficiency: 85% @ 12V. See attached data sheet.

Maximum Reverse Voltage: 25V

Maximum Reverse Current: 400μA

I-V Characteristics: See attached data sheet.

Pulse Response: See attached photo.

Diode Response vs Reverse Bias (273 MHz): See attached data sheet.

Note: Connect negative bias to the microdot connector.

Connect sampler head or current amplifier to the OSM connector.

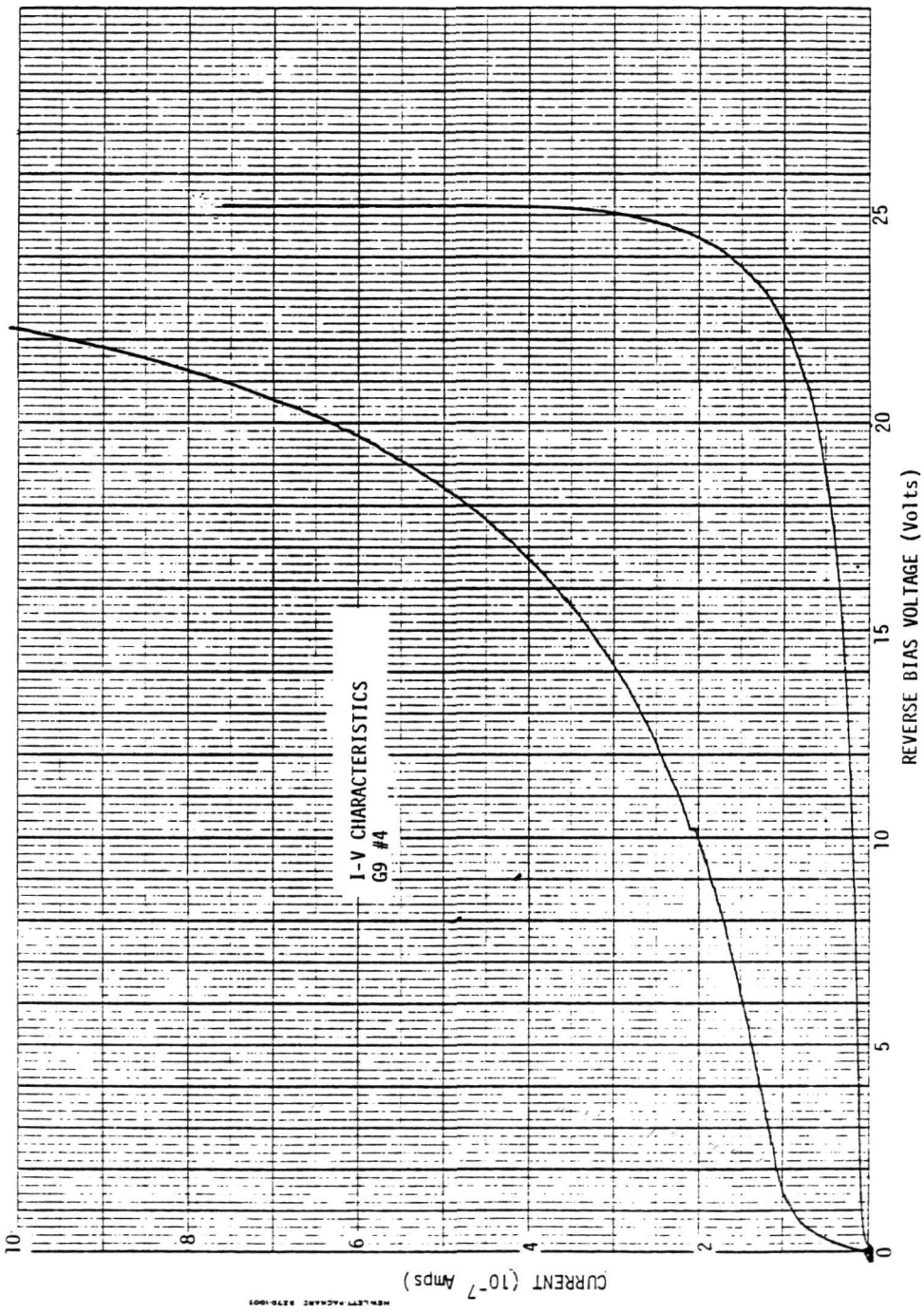
I-V CHARACTERISTICS
G9 #4
CURRENT (10^{-7} Amps)
REVERSE BIAS VOLTAGE (Volts)
0
2
4
6
8
10
5
10
15
20
25

Fig. A.11

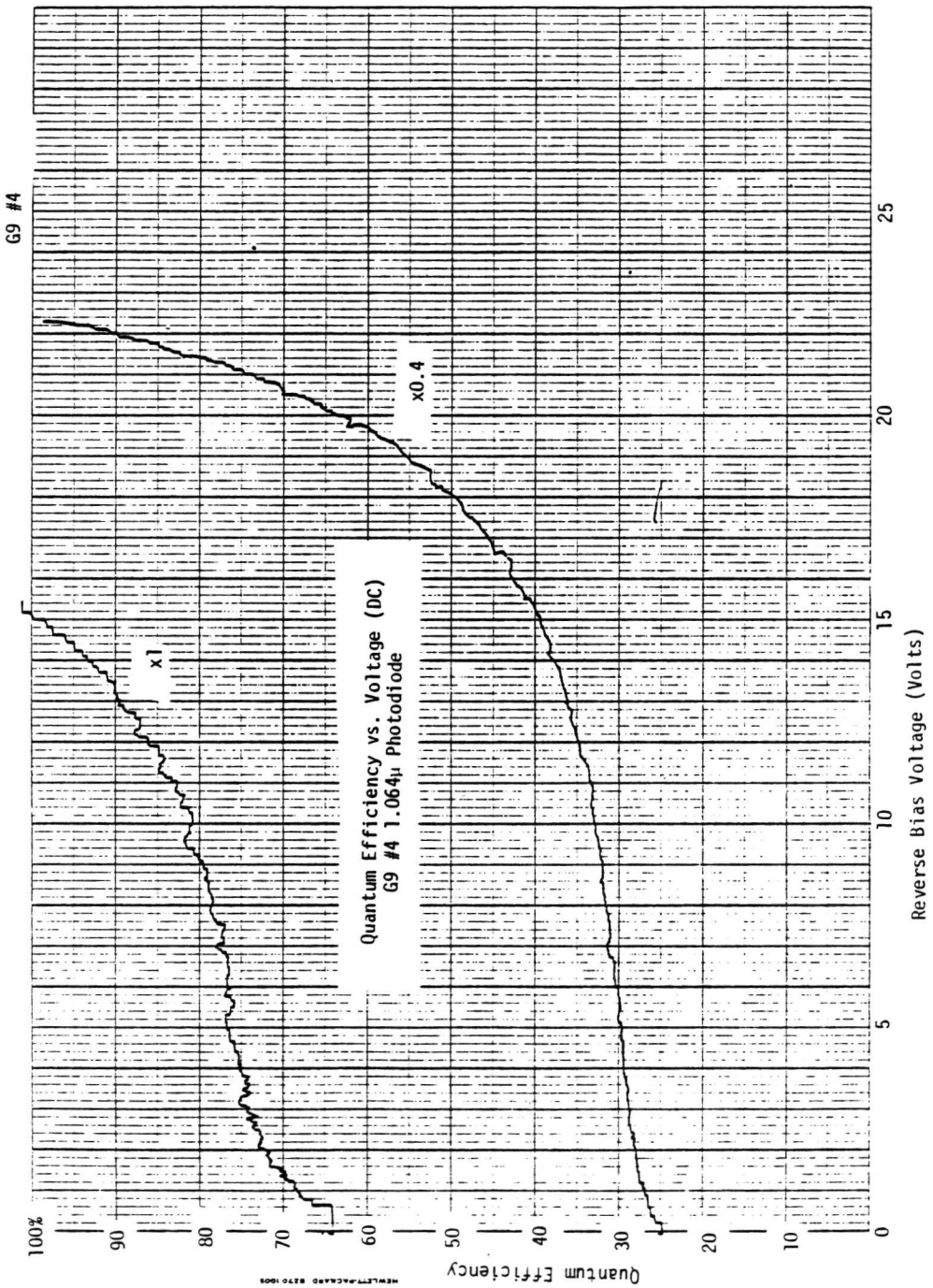
G9 #4
Quantum Efficiency vs. Voltage (DC)
G9 #4 1.064μ Photodiode
x1
x0.4
Quantum Efficiency
100%
90
80
70
60
50
40
30
20
10
0
0
5
10
15
20
25
Reverse Bias Voltage (Volts)

Fig. A.12

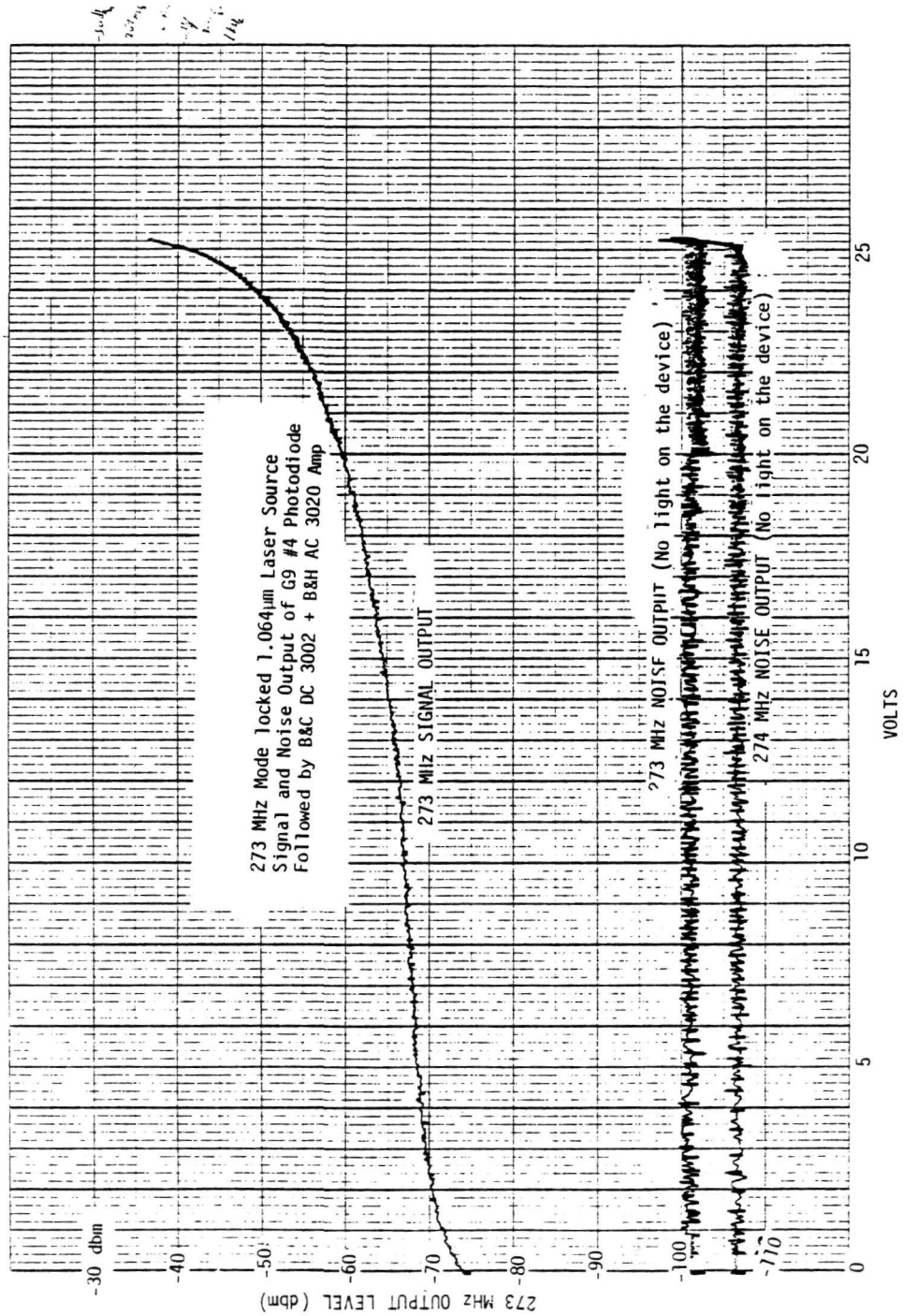
273 MHz Mode locked 1.064μm Laser Source
Signal and Noise Output of G9 #4 Photodiode
Followed by B&C DC 3002 + B&H AC 3020 Amp
273 MHz SIGNAL OUTPUT
273 MHz NOISE OUTPUT (No light on the device)
274 MHz NOISE OUTPUT (No light on the device)
273 MHz OUTPUT LEVEL (dbm)
-30 dbm
-40
-50
-60
-70
-80
-90
-100
-110
0
5
10
15
20
25
VOLTS

Fig. A.13

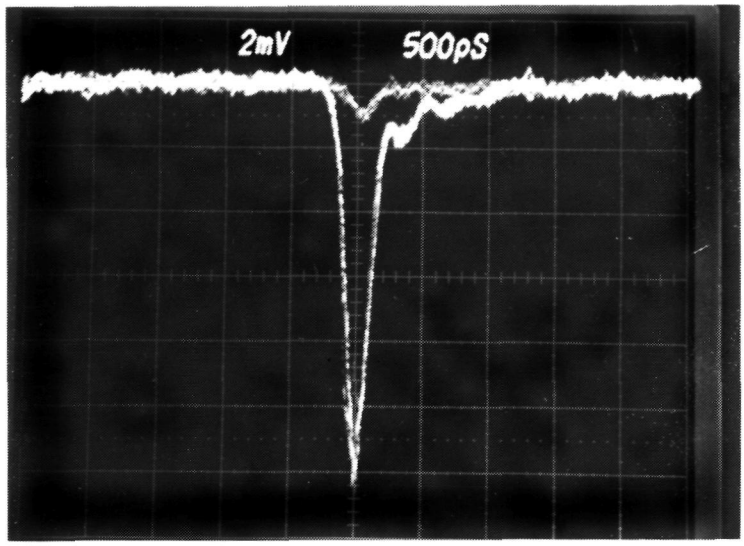

Fig. A.14 1.064μm mode locked laser pulse response for G9#4 diode. Upper curve 5V, 5 mV/div (vertical), 500 ps/div (horizontal); lower curve 25V, 5 mV/div (vertical), 500 ps/div (horizontal).